1. Extended Data

Complete the Inventory below for all Extended Data figures.

Figure #	Figure title One sentence only	Filename This should be the name the file is saved as when it is uploaded to our system. Please include the file extension. i.e.: *Smith_ED_Fig1.jpg*	Figure Legend If you are citing a reference for the first time in these legends, please include all new references in the Online Methods References section, and carry on the numbering from the main References section of the paper.
Extended Data Fig. 1	**Individual longitudinal changes of different phosphorylated-tau sites and total tau highlights differences in the time of increase relative to disease onset**.	McDade_ED_Fig1.jpg	Individual, z-transformed, longitudinal changes in the ratio of phosphorylation of **(a**) pT217/T217, **(b)** pT181/T181 **(c)** total tau, **(d)** pT205/T205, and **(e)** pS202/S202 for mutation carriers (orange = asymptomatic mutation carriers, (n= 152), red = symptomatic mutation carriers (n=77)) and non-carriers (blue, (n=141)) across the estimated years to symptom onset (EYO). The vertical dashed line is the point of expected symptom onset, the vertical green line represents the model estimated time when the rate of change for each p-tau isoform becomes greater for mutation carriers compared to non-carriers.
Extended Data Fig. 2	**Individual longitudinal changes of different unphosphorylated-tau sites**.	McDade_ED_Fig2.jpg	Individual, z-transformed, longitudinal changes in the unphosphorylated levels of **(a**) T217, **(b)** T181 **(c)** T205 for mutation carriers (orange = asymptomatic mutation carriers, (n= 152), red = symptomatic mutation

			carriers (n=77)) and non-carriers (blue, (n=141)) across the estimated years to symptom onset (EYO). The solid line represents a LOESS fit to cross-sectional and longitudinal data. The vertical dashed line is the point of expected symptom onset. Compared to the phosphorylation ratios of each site (Extended Data Fig 1), the increase in the unphosphorylated levels appears to be more similar over the progression of disease.
Extended Data Fig. 3	**Change in tau phosphorylation state is site dependent and related to amyloid PET and disease stage in DIAD and sAD.**	McDade_ED_Fig3.jpg	Bar charts illustrating the proportion of participants that have p-tau ratios and total tau levels that exceed the normal values (biomarker + (red)) (a- d) as the stage of disease progresses from cognitively normal/PiB-PET normal to cognitively normal/PiB-PET positive then to mild dementia (CDR 0.5) and greater (CDR > 0.5). The top row is DIAD (n = 210) and the bottom row sAD (n= 83). The figure demonstrates very similar patterns for each phosphorylation ratio and total tau levels across the progression of disease and indicate a similar ordering in DIAD and SAD, generalizing these findings to AD.
Extended Data Fig. 4	**Elevated levels of tau phosphorylation decline in some sites with atrophy of hippocampal volumes in contrast to a continued rise in total tau**.	McDade_ED_Fig4.jpg	Estimated individual annual rates of change of p-tau isoforms and total tau, standardized by the mean and standard deviation of the estimated rate of change for all mutation carriers, (y-axis) for mutation carriers were correlated with the annual change in hippocampal volumes (**a-d**). The linear regression was fit to those with no dementia (CDR 0, black circle, n= 48) and dementia (CDR >0, red triangle, n= 27). A decline in pT217/T217 (a), r= 0.74(p < 0.0001), pT181/T181 (b), r= 0.84 (p < 0.0001) and pT205/T205, r= 0.25 (p=0.03) phosphorylation rate was associated with hippocampal volume decline. For total tau there was an inverse correlation with atrophy (d), r= -

			0.79($p < 0.0001$). (e) A linear fit for all mutation carriers demonstrates there are distinct associations between declining cognition and changes in the different p-tau isoforms and total tau: with decreases in pT217/T217 and pT181/T181 and an increase in total tau associated with cognitive decline; and no associations with pT205/T205 or pS202/S202. This suggests that soluble tau species are not equivalent in AD (pS202/S202*)* is shown here to demonstrate the lack of association with cognition, r= -0.07 (p=0.57). Statistical significance of the correlations was calculated using z test.
Extended Data Fig. 5	**Elevated levels of tau phosphorylation decline in some sites with atrophy of precuneus cortex in contrast to a continued rise in total tau**.	McDade_ED_Fig5.jpg	Estimated individual annual rates of change of p-tau isoforms and total tau, standardized by the mean and standard deviation of the estimated rate of change for all mutation carriers, (y-axis) for mutation carriers were correlated with the annual change in hippocampal volumes (**a-d**). The linear regression was fit to those with no dementia (CDR 0, black circle, n= 48) and dementia (CDR >0, red triangle, n= 27). A decline in pT217/T217 (a), r= 0.75 (*p* <0.0001), pT181/T181 (b), r= 0.83 (*p* <0.0001) and pT205/T205, r= 0.19 (*p* = 0.09) phosphorylation rate was associated with precuneus cortical decline. For total tau there was an inverse correlation with atrophy (d), r= -0.77($p < 0.0001$). (e) A linear fit for all mutation carriers demonstrates there are distinct associations between declining cognition and changes in the different p-tau isoforms and total tau: with decreases in p-T217 and p-T181 and an increase in total tau associated with cognitive decline; and no associations with pT205/T205 or pS202/S202. This suggests that soluble tau species are not

			equivalent in AD (pS202/S202 is shown here to demonstrate the lack of association with cognition, r= -0.04 (*p* = 0.72). Statistical significance of the correlations was calculated using two-sided *t* tests.
Extended Data Fig. 6	**Tau PET increases near symptom onset in DIAD mutation carriers.**	McDade_ED_Fig6.jpg	The mean cortical standardized unit value ratio (SUVR), y-axis, for mutation carriers (red, n=12) and non-carriers (blue, n=9) over estimated years to symptom onset (EYO), x-axis, for those participants with a longitudinal CSF evaluation preceding the time of tau-PET. The plot shows that for mutation carriers there is little elevation in tau-PET until the point of estimated symptom onset (EYO =0). This figure shows that the neurofibrillary tangle (NFT) pathology detected by AV-1451 occurs much later than the increase in multiple soluble phosphotau sites suggesting that these soluble markers of tau are likely a marker of NFT pathology, but rather might predispose to the development of the hyperphosphorylated, insoluble tau deposits characteristic of AD pathology.
Extended Data Fig. 7	**Longitudinal change in tau and tau phosphorylation sites are differentially related to neurofibrillary tau (tau-PET) in dominantly inherited AD**.	McDade_ED_Fig7.jpg	Individual, rates of change of phosphorylation and total tau (y-axis) in mutation carriers only leading up to the time of tau-PET scan (x-axis) (n=12). The vertical line is an SUVR of 1.22 and represents a conservative estimate of the point when cortical tau-PET is considered elevated for tau aggregates compared to non-carriers. The plots suggest that increases in soluble tau and p-T205 are associated with higher levels of aggregated tau, whereas the rate of phosphorylation at p-T217 and p-T181 decrease as levels of aggregated tau increase. These findings suggest that there are differences between increasing levels of tau and phosphorylation at different sites and may indicate that, in some instances, soluble p-tau maybe

			sequestered as the burden of hyperphosphorylated aggregates increase with the spreading of tau pathology. They also suggest that with the increase in aggregated tau there is a rise in soluble tau levels which could represent either passive or active release with greater burden of aggregated tau pathology.
Extended Data Fig. 8	**Spearman correlation of the cross-sectional association of p-tau phosphorylation, total tau (y-axis) and tau PET (x-axis) for mutation carriers (n = 12).**	McDade_ED_Fig8.jpg	The vertical line is an SUVR of 1.22 and represents a conservative estimate of the point when cortical tau-PET is considered elevated for tau aggregates compared to non-carriers.
Extended Data Fig. 9			
Extended Data Fig. 10			

Delete rows as needed to accommodate the number of figures (10 is the maximum allowed).

2. Supplementary Information:

A. Flat Files

Complete the Inventory below for all additional textual information and any additional Supplementary Figures, which should be supplied in one combined PDF file.

Item	Present?	Filename This should be the name the file is saved as when it is uploaded to our system, and should include the file extension. The extension must be .pdf	A brief, numerical description of file contents. i.e.: *Supplementary Figures 1-4, Supplementary Discussion, and Supplementary Tables 1-4.*
Supplementary Information	Yes	McDade_SupplementaryFiles.pdf	Supplementary Tables 1-14
Reporting Summary	Yes	nr-reporting-summary_A97217	

17

18

19 ## B. Additional Supplementary Files

20

21 **Complete the Inventory below for all additional Supplementary Files**
22 **that cannot be submitted as part of the Combined PDF.**

23

24

Type	Number If there are multiple files of the same type this should be the numerical indicator. i.e. "1" for Video 1, "2" for Video 2, etc.	Filename This should be the name the file is saved as when it is uploaded to our system, and should include the file extension. i.e.: *Smith_Supplementary_Video_1.mov*	Legend or Descriptive Caption Describe the contents of the file
Choose an item.			
Choose an item.			
Choose an item.			

Choose an item.			
Choose an item.			
Choose an item.			

Add rows as needed to accommodate the number of files.

3. Source Data

Complete the Inventory below for all Source Data files.

Figure	Filename This should be the name the file is saved as when it is uploaded to our system, and should include the file extension. i.e.: *Smith_SourceData_Fig1.xls,* or *Smith_Unmodified_Gels_Fig1.pdf*	Data description i.e.: Unprocessed Western Blots and/or gels, Statistical Source Data, etc.
Source Data Fig. 1		
Source Data Fig. 2		
Source Data Fig. 3		
Source Data Fig. 4		
Source Data Fig. 5		
Source Data Fig. 6		
Source Data Fig. 7		
Source Data Fig. 8		
Source Data Extended Data Fig. 1		
Source Data Extended Data Fig.		

2		
Source Data Extended Data Fig. 3		
Source Data Extended Data Fig. 4		
Source Data Extended Data Fig. 5		
Source Data Extended Data Fig. 6		
Source Data Extended Data Fig. 7		
Source Data Extended Data Fig. 8		
Source Data Extended Data Fig. 9		
Source Data Extended Data Fig. 10		

A soluble phosphorylated tau signature links tau, amyloid and the evolution of stages of dominantly inherited Alzheimer's disease

Nicolas R. Barthélemy[1], PhD, Yan Li[1,2], PhD, Nelly Joseph-Mathurin[3], PhD, Brian A. Gordon[3], PhD, Jason Hassenstab[1], PhD, Tammie. L.S. Benzinger[3], MD, PhD, Virginia Buckles[1], PhD,

Anne M. Fagan[1], PhD, Richard J. Perrin[4], MD, Alison M. Goate[5], PhD, John C. Morris[a], MD, Celeste M. Karch[6], PhD, Chengjie Xiong[2], PhD, Ricardo Allegri[7], Patricio Chrem Mendez, MD[7], Sarah B. Berman[8], MD, PhD, Takeshi Ikeuchi[9], MD, PhD, Hiroshi Mori[10], PhD, Hiroyuki Shimada[10], MD, PhD, Mikio Shoji[11], MD, PhD, Kazushi Suzuki[12], MD, PhD James Noble[13], MD, Martin Farlow[14], MD, Jasmeer Chhatwal[15], MD, Neill R. Graff-Radford[16], Stephen Salloway[17], MD, Peter R. Schofield[18,19], MD, Colin L. Masters[20], MD, Ralph N. Martins[21] PhD, Antoinette O'Connor[22], MD, Nick C. Fox[22], MD, Johannes Levin[23,24,25], MD, Mathias Jucker[26,27], PhD, Audrey Gabelle[28], MD,PhD, Sylvain Lehmann[28], MD, Chihiro Sato[1], PhD, Randall J. Bateman[1*], MD, Eric McDade[1*], DO and the Dominantly Inherited Alzheimer Network

Author affiliations:

[1]Department of Neurology, Washington University School of Medicine, Saint Louis, MO, USA

[2]Division of Biostatistics, Washington University School of Medicine, Saint Louis, MO, USA

[3]Department of Radiology, Washington University School of Medicine, Saint Louis, MO, USA

[4] Department of Pathology, Washington University School of Medicine, Saint Louis, MO, USA

[5]Department of Neuroscience, Icahn School of Medicine at Mount Sinai, New York, NY, USA

[6]Department of Psychiatry, Washington University School of Medicine, Saint Louis, MO, USA

[7]Fundación para la Lucha contra las Enfermedades Neurológicas de la Infancia (FLENI) Instituto de Investigaciones Neurológicas Raúl Correa, Buenos Aires, Argentina,

[8]University of Pittsburgh School of Medicine, Pittsburgh, PA, USA

[9]Niigata University, Niigata, Japan

[10]Osaka City University, Osaka, Japan

[11]Hirosaki University, Hirosaki, Japan

[12]Tokyo University, Tokyo, Japan

[13]Columbia University, College of Physicians and Surgeons, NY, NY, USA

[14]Department of Neurology, Indiana University, Indianapolis, IN, USA

[15]Massachusetts General Hospital, Harvard Medical School Boston, MA, USA

[16]Department of Neurology, Mayo Clinic Jacksonville, Jacksonville, FL, USA

[17]Butler Hospital and Brown University, Providence, RI, USA

[18]Neuroscience Research Australia, Sydney, , Australia

[19]School of Medical Sciences, University of New South Wales, Sydney, , Australia

[20]The Florey Institute and the University of Melbourne, Parkville, , Australia

[21]Edith Cowan University, Perth, Nedlands, Western Australia

[22]Dementia Research Centre, Institute of Neurology, University College London, London, UK

[23]German Center for Neurodegenerative Diseases (DZNE) Munich, Munchen, Germany

[24]Department of Neurology, Ludwig-Maximilians Universität München, Munich, Germany

[25]Munich Cluster for Systems Neurology (SyNergy), Munich, Germany

[26]German Center for Neurodegenerative Diseases (DZNE) Tübingen

[27]Hertie-Institute for Clinical Brain Research, University of Tübingen, DTübingen, Germany

[28]CHU Montpellier, IRMB, hˆopital St Eloi, Laboratoire de Biochimie Prot´eomique Clinique et CRB, INSERM-UM, Montpellier, France

***Co-Correspondence:**
Dr. Eric McDade and Dr. Randall J. Bateman
Washington University School of Medicine,
Department of Neurology,
660 S. Euclid Ave., Box 8111,
St. Louis, MO 63110,
ericmcdade@wustl.edu, batemanr@wustl.edu

Abstract:

Development of tau-based therapies for Alzheimer's disease requires an understanding of the timing of disease-related changes in tau. We quantified the phosphorylation state at multiple sites of the tau protein in cerebrospinal fluid markers across four decades of disease progression in dominantly inherited Alzheimer's disease. We identified a pattern of tau staging where site-specific phosphorylation changes occur at different periods of disease progression and follow distinct trajectories over time. These tau phosphorylation state changes are uniquely associated with structural, metabolic, neurodegenerative and clinical markers of disease and some (p-tau217 and p-tau181) begin very early with the initial increases in aggregate amyloid-β as early as two decades prior to development of aggregated tau pathology. Others (p-tau205 and t-tau) increase with atrophy and hypometabolism closer to symptom onset. These findings provide insights into the pathways linking tau, amyloid-β, and neurodegeneration and may facilitate clinical trials of tau-based treatments.

The microtubule-associated protein tau (MAPT or *tau*) plays an essential role in the morphology and physiology of neurons[1,2]. Phosphorylation is an important post-translational modification for regulating the normal function of tau in axonal stabilization and can occur at over 80 different positions[3]. However, excessive phosphorylation of tau (p-tau) appears to increase the probability of tau aggregating into intracellular insoluble paired helical filaments (PHF) and neurofibrillary tangles (NFT)[4,5], which are primarily composed of hyperphosphorylated tau. Intracellular neurofibrillary tangles in the cerebral cortex are a defining pathological feature of Alzheimer's disease (AD) and correlate with the onset of clinical symptoms long after the appearance of extracellular aggregated amyloid-β (Aβ) 'plaques'[6,7], which begin to develop up two decades before symptom onset[8,9]. In AD, soluble p-tau181 (pT181) and unphosphorylated total tau (t-tau) are elevated in the cerebrospinal fluid (CSF)[10-12] and begin to increase prior to symptom onset in both dominantly inherited AD (DIAD) and sporadic AD (sAD)[13,14]. It has been proposed that these changes reflect the effects of neuronal death (neurodegeneration) passively releasing tau and NFT[15,16] into the CSF. However, in other tauopathies with significant NFT pathology and neurodegeneration (e.g. progressive supranuclear palsy, frontotemporal lobar degeneration-tau), CSF levels of soluble pT181 and t-tau do not increase[17,18] and in AD, NFTs as measured by tau positron emission tomography (tau-PET) only modestly correlate with CSF t-tau and p-tau[19,20]. Moreover, recent work in DIAD and sAD has suggested that NFT, as measured by tau-PET, primarily increases at symptom onset 10-15 years after[21-25] soluble tau increase[26-28]. Further, the rate of the increase of p-tau and tau levels may actually slow as neurodegeneration increases[8,13,29]. These observations suggest that the tauopathy of AD is a more dynamic process than currently conceptualized[15], soluble and aggregated tau likely have important differences and that cerebral Aβ may trigger a process that leads to the unique tauopathy of AD[22,30-38]. This

concept is further supported by an increase in the active production of soluble tau in the presence of aggregated amyloid in humans[34]. ^{11}C-Pittsburgh compound B (PiB) PET imaging of cortical aggregated Aβ has detected Aβ pathology two decades before the appearance of symptoms in DIAD[8,39], but has not consistently been linked with a rise in CSF tau and pT181[8]. However, unresolved questions include: 'What is the relationship of tau to aggregated Aβ?' and 'What are the different tau pathophysiologic changes that occur during the preclinical and clinical stages of AD?'. The answers to these questions will help identify the tau pathophysiologic processes that are related to AD and neurodegeneration, which is a critical step needed to advance therapeutic and diagnostic targets for the disease.

An important limitation to understanding the tauopathy of AD has been the lack of methods that can simultaneously quantify phosphorylation at multiple positions of the tau protein in a population representing the full clinicopathological spectrum of AD – at risk through dementia. To further explore these questions and limitations we developed a mass spectrometry (MS) method to measure the phosphorylation occupancy (phosphorylated to unphosphorylated) at multiple tau phosphorylation sites in the proline-rich protein domain ranging from 150 to 220 residues[34] in CSF, independent of variation in total tau levels. We measured CSF from a large cohort of comprehensively-studied participants with DIAD (n= 370), as well as cohort of sAD and cognitively normal adults at risk (based on the presence of abnormal Aβ pathology) (n= 104), (Table 1 and Supplemental Table 1), and quantified multiple positions throughout tau and the associated phosphorylation occupancy in order to determine disease stage-specific changes in soluble p-tau isoforms. The relatively predictable age of disease onset in DIAD families[40] enables us to infer the pattern of change across decades of AD progression. This cohort was recruited and evaluated by the Dominantly Inherited Alzheimer Network (DIAN), a global,

multi-site, observational study of adults with and at-risk of carrying causative mutations for early onset AD. Participants undergo a comprehensive, standardized assessment of biofluids, brain imaging, cognitive and clinical assessments.

The results of our investigation show that hyperphosphorylation at specific sites of the tau protein is a dynamic process that changes first based on the pathological state (i.e. presence and amount of aggregated Aß), then stage of disease, and clinical stage (cognitively normal or cognitively impaired) of AD in both DIAD and sAD. Further, in DIAD we demonstrate that these phosphorylation sites have opposite trajectories of change at different stages over the 30 years of the DIAD process and have different associations with brain hypometabolism, atrophy and cognitive decline (Fig 1). These findings suggest a predictable progression of changes in tau phosphorylation- an AD-tau staging system- and support recent tau kinetic studies demonstrating aggregated Aß related active release of phosphorylated tau[34]. Moreover, this AD-tau staging suggests potential tau targets for development of tau-specific therapeutics and provides down-stream measures for therapies targeting early amyloid pathology.

Insert Figure 1 here

Results

Disease stage and progression are associated with site-specific differences in tau hyperphosphorylation and longitudinal rates of change in DIAD and sAD

The certainty of disease and predictability of symptom onset of DIAD enables the staging of individuals based on anestimated years to symptoms onset (EYO) [8,27,41] (i.e. the age of an individual at the time of assessment relative to the age of onset of others with the mutation). Therefore, we determined whether there were temporal differences in the pattern of

187 phosphorylation of CSF tau as it relates to the estimated year to symptom onset. This was done
188 by estimating the differences in the amount and rate of change in phosphorylation over time
189 between MCs and NCs based on EYO. There were two important findings. First, there was
190 evidence that increases in total tau and phosphorylation at specific sites occurred in a relative
191 order: Phosphorylation of tau at threonine 217 (pT217/T217) (which occurred around -21 EYO)
192 was followed by that of threonine 181 (pT181/T181) (-19 EYO), then total tau increase (-17
193 EYO), then at threonine 205 (pT205/T205) (-13 EYO) **(**Fig. 2, and Extended Data Fig. 1a-e and
194 Supplemental table 2**).** The initial increase of pT217/T217, and to a lesser extent in pT181/T181,
195 occurred at a similar time to when PiB-PET SUVR began to increase (-19 EYO), (see below).

196 **Insert Table 1 and Figure 2 here**

197 Second, pT217/T217 and pT181/T181 began to decline significantly near the time of symptom
198 onset, while phosphorylation at pT205/T205 slowed and total tau levels continued to increase. Of
199 note, the concentration of all the corresponding unphosphorylated isoforms (T181, S202/T205,
200 T217) increased with disease progression suggesting that the decrease in the phosphorylation
201 ratio for pT217/T217 and pT181/T181 was not a result of a disproportionate rise in
202 unphosphorylated peptides specifically related to these two sites, nor a decrease in total levels of
203 tau protein **(**Extended Data Fig 2). For phosphorylation at the 202 position of serine
204 (pS202/S202) there was no significant change in phosphorylation over the course of the disease
205 (Fig. 2, Extended Data Fig 2c).

206 Next, we assessed whether the above findings were also seen in an elderly group of patients with
207 sAD and non-mutation carriers that are at risk for AD based on the presence of abnormal Aβ
208 biomarkers- preclinical AD (n = 63), or those with normal Aβ biomarkers (n = 39). This group of

participants underwent clinical assessments - the Clinical Dementia Rating scale (CDR), CSF collection and Aβ measures cross-sectionally. Because sAD is associated with a later age and additional pathologies (e.g. vascular disease, TDP-43) compared with a more 'pure' form of AD in DIAD it is possible that there could be important differences in tau phosphorylation between the two types of AD. However, preclinical sAD population lacks a predictor of disease onset like EYO in DIAD and did not have longitudinal CSF, therefore, we compared the two groups based on 1) the absence or presence of amyloid pathology (to define a similar AD risk state) and 2) the stage of dementia symptoms using the CDR (CDR 0- no dementia, CDR 0.5- very mild dementia, CDR >= 1- mild to moderate dementia)[42] (Fig 3c).

Insert Figure 3 here

Overall, there was a similar pattern of phosphorylation changes at each site for both cohorts. In both DIAD and sAD pT217/T217 and pT181/T181 ratios increase significantly with the presence of amyloid pathology and then less so with more advanced stages of symptoms. However, for pT205/T205 and total tau the rate of phosphorylation and increase in levels of tau increase at later stages and continue increasing as clinical disease progresses. Similarly, in both DIAD and sAD, the phosphorylation of p-S202 remains relatively stable with amyloid pathology and disease progression. Notably, there was evidence that in DIAD there was a greater magnitude of phosphorylation and higher levels of total tau for each category compared to sAD.

We next evaluated the proportion of participants in both cohorts that exceeded the values considered abnormal for t-tau and each phospho-tau isoform for each category of PiB-PET (positive or negative) and clinical progression (CDR 0, 0.5 or >=1). Extended Data Fig. 3 and Supplemental Table 3 demonstrate very similar patterns for DIAD and sAD as it relates to the

sequential increases in phosphorylation at pT217/T217 and pT181/T181 first, coinciding with the presence of PiB-PET amyloid, followed by increases in pT205/T205 and total tau with the development and progression of clinical symptoms.

These results indicate that phosphorylation of tau changes at specific sites by disease stage. In DIAN, in particular, this suggests a cascade of changes in soluble tau that is more dynamic than previously realized, and that tau does not monotonically increase in phosphorylation states or rates. The emergence of PiB-PET Aβ and the onset of clinical decline, separated by nearly two decades, mark two important stages of soluble tau phosphorylation changes in DIAD and sAD and suggests that the two different pathways to AD have a similar pattern of evolution in the abnormal processing of tau and expression in the CSF.

Cerebral amyloid pathology is associated with site-specific differences in tau hyperphosphorylation in presymptomatic DIAD

Given the temporal sequence of changes in tau species identified using disease predictability (EYO), we then sought to determine if changes in other biomarkers across the disease could reveal important associations with the different sites of phosphorylation in DIAD. To explore the relationship of aggregated Aβ and soluble tau phosphorylation, we compared the SUVR value of cortical PiB-PET that reliably identifies significant brain aggregated Aß (SUVR >1.25) with the phospho-tau isoforms to determine concordance with aggregated Aß (*Amyloid* +, SUVR ≥ 1.25 or *Amyloid* -, SUVR < 1.25) (Fig. 3a). pT217/T217 had a 97.2% area under the curve (AUC) (95% Confidence Interval (CI) of 0.94, 0.99); pT181/T181 had an 89.1% AUC (CI 0.83, 0.94); pT205/T205 had a 74.5% AUC (CI 0.69, 0.82); total tau had a 72% AUC (CI 0.65, 0.79); at the 202 position of serine (pS202/S202) had a 69% AUC (CI 0.62, 0.77) to classify asymptomatic

253 participants as having PiB-PET SUVR levels consistent with aggregated Aβ. This indicates that
254 at the early stages of significant fibrillar Aβ plaques, an increase of phosphorylation has already
255 begun at specific positions linking these two processes in time and also demonstrates that an
256 increase in the phosphorylation occupancy on T217 could serve as a sensitive diagnostic marker
257 for aggregated Aβ plaque pathology measured by PiB-PET, identifying a potentially unique
258 signature of Aβ-related tau processing in DIAD. When using CSF soluble Aβ in DIAD to
259 determine abnormal amyloid levels we found the same order for the soluble tau measures in
260 classifying participants as Amyloid + (Aβ 42/40 ≥ 0.0776) or - (Aβ 42/40 < 0.0776), but lower
261 AUC values for each (Supplemental Table 4**)**. Additionally, we compared this mass spectrometry
262 (MS) based method to one of the most advanced immunoassays (Roche Elecsys® p-tau181 and
263 total tau CSF electrochemiluminescence method) and found the MS method to be superior,
264 indicating a greater sensitivity to detecting early AD pathology in DIAD **(**Supplemental Table 5**)**.

265 We then compared the ratios (standardized to a z-score across all mutation carriers (MC)) at four
266 phosphorylation sites and total tau levels by PiB-PET SUVR quartiles to explore the cross-
267 sectional relationship between total aggregated Aβ load and phosphorylation (Fig. 3b). All
268 phosphorylation sites except at S202 demonstrated increased levels of phosphorylation with
269 greater PiB-PET SUVR; in contrast, pS202/S202 had a decrease in phosphorylation with
270 increasing PiB-PET SUVRs. These results suggest that the events initially leading to increased
271 tau phosphorylation in AD are likely related to aggregated Aβ pathology, potentially through
272 regulation by distinct kinases and phosphatases that are phosphorylation site specific[43]. Yet, as
273 aggregated Aβ burden continues to increase, there are differences between the amount of
274 phosphorylation that continues to occur among different p-tau isoforms. Importantly, among

mutation non-carriers (NCs), the only participants who showed an increase in pT217/T217 were those who were Amyloid+ (SUVR > 1.25, n=4).

We next assessed whether phosphorylation of tau was associated with the anatomical distribution of cerebral aggregated Aβ pathology by exploring the cross-sectional correlations between the baseline p-tau phosphorylation sites and cortical and sub-cortical regions of amyloid plaque deposition as measured by PiB-PET SUVR in the a*symptomatic* MCs (Fig. 3d and Supplemental Table 6). Phosphorylation pT217/T217, pT181/T181, and pT205/T205 was positively correlated with PiB-PET SUVR throughout the brain, but pS202/S202 was negatively correlated. In the precuneus, a region of early amyloid plaque deposition[39], correlations with tau phosphorylation were compared based on the strength of bivariate regression controlling for age, gender, and estimated years to symptom onset (EYO) and adjusted for multiple comparisons. We found an order of correlations from greatest to least of pT217/T217 (r =0.53, s.e.m- 0.06, $p < 10^{-30}$), pT205/T205 (r =0.37, s.e.m- 0.075, $p < 10^{-5}$), pT181/T181 (r =0.35, s.e.m- 0.075, $p < 10^{-6}$), with positive correlations with PiB-PET SUVR. In contrast, pS202/S202 had an inverse correlation (r =-0.46, s.e.m- 0.067, $p < 10^{-7}$), suggesting that phosphorylation at this site is reduced with increasing aggregated Aβ pathology. We found a found a similar rank ordering for nearly all regions of PiB-PET and p-tau isoform correlations and statistically significant differences between the different p-tau measures correlations, most commonly for pT217/T217 having the greatest associations.

Neuroimaging markers of disease progression are associated with site- specific differences in tau hyperphosphorylation in presymptomatic DIAD

In addition to estimating the onset of symptoms using EYO, disease advancement in DIAD can also be estimated using neuroimaging measures that track various components of disease progression, e.g. brain atrophy and metabolic decline. These measures have been shown to change at different periods of time before symptom onset in DIAD, with declining cerebral metabolism (measured by [F18] fluorodeoxyglucose [FDG]-PET) occurring up to 18 years and brain atrophy (determined by MRI) occurring up to 13 years before symptom onset [39,44-46]. This raises the question of whether these biomarkers are likewise correlated with tau phosphorylation at specific sites. To examine this, we performed bivariate cross-sectional correlations between the phosphorylation sites and total tau with imaging measurements from 34 cortical and 6 subcortical brain regions, controlling for sex, age and EYO. We focused the analyses on asymptomatic MCs in order to identify any associations at the earliest stages of disease progression, prior to severe neurodegeneration. The phosphorylation state of pS202/S202 was not included in these analyses given its relative lack of change over disease progression.

MRI

Hyperphosphorylation was inversely associated with cortical thickness in asymptomatic MCs: pT205/T205, and slightly less pT217/T217, was most strongly associated with a decrease in cortical and subcortical thickness throughout the brain (Fig. 4a, Supplemental Table 7), while total tau levels showed fewer regional associations and weaker correlations. Hyperphosphorylation at pT181/T181 had the lowest overall correlation with cortical atrophy, restricted to the medial and lateral parietal lobes and medial dorsal-medial frontal lobes. This suggests that the initial rise in pT205/T205 at -13 EYO may be related to the underlying process of cortical atrophy, which we have previously shown to begin approximately at -13 EYO in the precuneus[39]. Previous work in DIAN and other DIAD cohorts has demonstrated that significant

atrophy as measured by MRI does not occur until closer to disease onset which would indicate that although an increase in CSF tau and phosphorylated tau may be in part related to a passive release in neurodegeneration their initial rise is likely the consequence of other processes.

Insert Figure 4 here

FDG PET

In addition to cortical atrophy, a decline in glucose metabolism in neurons and glia is associated with disease progression in AD. Therefore, we tested whether there were distinct associations between cortical or subcortical metabolic impairment and tau phosphorylation. In the asymptomatic MCs, phosphorylation at pT205/T205 was correlated with glucose hypo-metabolism throughout the cortex and sub-cortical regions, as measured by FDG-PET (Fig. 4b, supplemental Table 8**).** There were minimal associations identified for the other p-tau sites or total tau level in asymptomatic MCs.

Together, these results indicate that the underlying processes leading to neuronal impairment and neurodegeneration during asymptomatic disease progression, as measured by neuroimaging, have different associations to tau phosphorylation with pT205/T205 most strongly correlated with both.

Cognitive decline and brain atrophy are associated with site-specific differences in tau hyperphosphorylation in DIAD

Prior studies have shown that AD dementia is more closely related to neocortical NFT pathology than neocortical Aβ pathology[47], yet the relationship between soluble tau and cognition remains uncertain[48]. Therefore, we assessed the longitudinal change in the soluble tau phosphorylation

ratio and total tau levels over time in comparison to clinical outcomes[49]. We performed a mixed effect model with longitudinal cognitive performance on the neuropsychological composite as the outcome and annual change in CSF tau measures (derived from individual linear mixed effects models), time, and their interactions as the predictors, adjusting for age, sex, education, and familial relation (participants of the same family). We tested all MCs (symptomatic and asymptomatic) for this analysis in order to include a stage of the disease with significant cognitive decline and found differential effects between phosphorylation site and cognitive decline. t-tau monotonically increased with worsening cognition and pT217/T217 and pT181/T181 decreased with worsening cognition, while pT205/T205 demonstrated less change relative to cognitive decline and pS202/S202 having no association with cognitive change. As pT217/T217 and pT181/T181 decreased, cognitive decline accelerated (t value 2.35, $p = 0.02$ and 2.11, $p = 0.04$) (Fig. 5 Supplemental Table 9). For asymptomatic (CDR 0) participants there was evidence that an increase in pT181/T181, pT205/T205 and total tau levels was associated with the initial decline in cognition. This suggests that decreased phosphorylation of T217 and T181, as much as increased soluble t-tau, presents an important marker of cognitive decline. We also evaluated the longitudinal change in the soluble tau phosphorylation ratio and total tau levels over time in comparison to longitudinal MRI measures of neurodegeneration -atrophy of hippocampi and precuneus cortex- and found very similar results to those of cognition (Extended Data Fig 4-5). This further supports the finding that a decrease in the rate of phosphorylation of certain sites of tau represent an important marker of neurodegeneration and symptomatic disease progression.

Insert Figure 5 here

These findings provide a modification to the current paradigm that a continuous rise in CSF tau phosphorylation is associated with cognitive dysfunction. We identified two general patterns: for some sites, phosphorylation decreased significantly as cognitive decline began, whereas other sites showed a continuous increase or no change with disease progression (see increasing vs. decreasing rates in Fig 5).

Increasing levels of total tau are correlated with baseline cortical NFTs by tau PET in DIAD

Recent tau-PET (^{18}F AV-1451, or flortaucipir) studies with DIAD participants have suggested that aggregated tau (tau-PET) increase occurs following the onset of clinical symptoms[21,25]. We tested the hypothesis that soluble p-tau is a marker of NFT pathology. We explored the relationship between longitudinal change of CSF t-tau and p-tau isoforms leading up to the time when tau- PET was performed to assess if faster changes of phosphorylation ratios was associated with higher tau-PET SUVR (greater aggregated tau). In a limited number of participants (10 MCs and 4 NCs), a single tau- PET scan was performed within 72 hours of the CSF sample being obtained. For these individuals, CSF samples had also been obtained on previous visits (within 1-3 years).

First, we confirmed that tau-PET SUVR in MCs only increased near the time of symptom onset (Extended Data Fig 6)**,** suggesting that in DIAD MCs, clinical decline begins when tau-PET signal starts to increase. Second, we found that a longitudinal increase in CSF total tau leading up to the time of tau-PET was associated with an elevated global cortical tau-PET composite ($p = 0.05$) value (Supplemental Table 10) and that this association was related to multiple posterior and limbic cortical regions. Similarly, when exploring the Spearman correlation of the rate of change of soluble tau measures and baseline tau-PET SUVR we found evidence of increasing t-

tau (r= 0.58, p = 0.08) but also pT205/T205 (r=0.74, p = 0.02) were associated with higher tau-PET levels, whereas there was a suggestion of a decrease in pT217/T217 (r= -0.2, p = 0.58) and pT181/T181 (r= -0.27, p= 0.46) with higher tau-PET levels **(**Extended Data Fig 7 and Supplemental table 11). Given the small number of participants available for this analysis there are limits to the interpretation of these results. However, by measuring multiple sites of phosphorylation simultaneously these preliminary findings do illustrate that the increases of soluble phosphorylated tau identified in DIAD, and presumably in sAD, are not necessarily a reflection of increases in aggregated tau as measured by tau-PET. In contrast, these results might suggest that a reduction of the phosphorylation rate of some sites (e.g. p-tau181 and p-tau217) when aggregated tau is increasing could represent a process of sequestration by hyperphosphorylated aggregates[50].

Discussion

Although aggregated tau is a hallmark of AD pathology important gaps remain in our understanding of how phosphorylation leads to the development of NFTs[2] and neurodegeneration in humans. Here we demonstrate how patterns of tau phosphorylation in the CSF of DIAD mutation carriers vary over the course of AD progression. We add to the existing clinical literature the demonstration that in DIAD, the process of tau phosphorylation and release into the CSF is a dynamic process that: 1) begins once aggregated Aβ pathology (as measured by PiB-PET) is established decades prior to symptoms, and subsequently unfolds over a period of nearly two decades; 2) occurs in a pattern such that phosphorylation of different tau sites closely follows disease progression as revealed by levels of other biomarkers; and 3) decreases significantly in a site-dependent manner near the onset of cognitive decline and the rise in aggregated tau (as measured by tau-PET). Together, these results indicate that this method of

quantifying soluble tau phosphorylation occupancy can track the AD process across its preclinical to symptomatic stages, providing a signature of phospho-tau pathology in this disease (Supplemental Table 12). Moreover, they challenge the purported roles of tau/p-tau in DIAD, and possibly AD in general, and recapitulate in humans those findings from animal studies that link Aβ pathology to tau hyperphosphorylation[33,35,37,51] and active cellular release rather than a consequence of release of dying neurons.

Although causality needs to be addressed in future studies, the contemporaneous increases in pT217/T217, pT181/T181 and PiB-PET SUVR suggest that the phosphorylation of tau in AD is closely linked to Aβ pathology. This is consistent with recent work in AD transgenic mice[32,33,35,52,53] and in humans which demonstrate that tau and hyperphosphorylated tau is released from cells in an active process that is increased in the presence of aggregated Aβ[34]. Our results link Aβ pathology to a distinct change in soluble tau level and phosphorylation patterns, shedding light on the phenomenon in which significant elevation of p-tau occurs in AD but not in other neurodegenerative tauopathies.[17,18]

Recent work has shown an increase and spread of neuritic tau aggregates (PHFs in dystrophic neurites) in Aβ transgenic mice is enhanced by the presence of aggregated Aβ, occurring before established somatic NFTs[32]. It is possible that the very early increase we find in pT217/T217 and pT181/T181 may reflect this "early" tau response to aggregated Aβ and might explain the global association of PiB-PET SUVR with these isoforms that we identified. Additionally, the lack of clinical symptoms seen during this early elevation in phosphorylation of tau suggests it occurs years before the onset of significant neurodegeneration. Our findings of an increase in pT205/T205 being associated with a decline in synaptic homeostasis could represent a protective process resulting in increased phosphorylation at T205 with synaptic distress from chronic Aß

exposure, at least in DIAD[53]. Importantly, we have shown that the t-total levels appears to rise to similar levels with disease progression, supplemental Fig. 2. This would indicate that the differences we have detected in the phosphorylation occupancy in DIAD are less likely to just reflect a difference in the amount of intraneuronal tau protein produced and released into the CSF compartment. Rather, it might suggest that with different stages of the disease, Fig. 1, there are unique activations of the different kinases responsible for phosphorylating the tau protein preferentially at specific sites[43].

These data call into question some common assumptions about the role of soluble tau and p-tau in AD. Specifically, the current diagnostic framework in AD emphasizes the presence of biomarkers representing AD specific and non-specific pathologies (e.g. Aβ, p-tau and tau)[15]. Within this diagnostic framework, soluble p-tau and t-tau are often presumed to be passively released from degenerating neurons, with p-tau associated with aggregated NFTs and t-tau associated with axonal degeneration. Cross-sectional associations between phosphorylation levels and tau-PET in prior studies and our own data (Extended Data Fig 8 and Supplemental Table 13) suggested that soluble phosphor-tau and aggregated tau by tau PET are correlated. In contrast, the more appropriate longitudinal measures indicate that soluble tau phosphorylation occupancy decreases during the time of tau-PET increase[25], at least in DIAD, demonstrating an *inverse-correlation*. One possible explanation for this is similar to what has been observed with soluble/aggregated Aβ[54]: that the dramatic increase of aggregated tau sequesters phosphorylated tau[55] in the brain, decreasing CSF levels. In addition, early phosphorylation modifications, suggest that hyperphosphorylation, although a marker of pathophysiology, is not necessarily a marker of tau-related NFTs.

A reduction of tau through proteostatic mechanisms cannot be excluded[56] as a cause for the decrease in phosphorylation but the continued increase of t-tau, supplemental figure 3, would suggest that this is not likely the cause for the decreasing rate of phosphorylation for some sites. Similarly, a recent study has demonstrated that the new production of tau and levels in the CSF does not appear to change in the presence of elevated tau-PET[34]. In either case, our findings of the negative correlation between the phosphorylation ratios of pT217/T271 or pT181/T181 and longitudinal cognitive decline and MRI measures of neurodegeneration highlights the importance of the reversal in phosphorylation rate of some tau sites in disease progression. Elucidating the cause for this decline could lead to a better understanding of the links between soluble tau and neuronal dysfunction and the use of CSF p-tau/tau in AD prognostication.

In summary, we have now demonstrated that in AD associated with autosomal dominant mutations, CSF tau hyperphosphorylation occurs very early and exhibits pattern of site-specific changes at different stages of the disease. The underlying mechanisms behind these findings will have important implications understanding the disease and for tau-directed therapies for AD.

Acknowledgments: *Data collection and sharing for this project was supported by The Dominantly Inherited Alzheimer's Network (*DIAN, UF1AG032438*) funded by the National Institute on Aging (NIA), the German Center for Neurodegenerative Diseases (DZNE), Raul Carrea Institute for Neurological Research (FLENI), Partial support by the Research and Development Grants for Dementia from Japan Agency for Medical Research and Development, AMED, and the Korea Health Technology R&D Project through the Korea Health Industry Development Institute (KHIDI), MRC Dementias Platform UK (MR/L023784/1 and*

MR/009076/1), AOI Lady Biobank CHU. The development and performance of the mass spectrometry analyses was supported by the Alzheimer's Association Research Fellowship (AARF-16-443265, N.R.B.), Fondation Du Plan Alzheimer (AG, SL), BrightFocus (A20143845, R.J.B.), the National Institute of Neurological Disorders and Stroke (R01NS095773, R.J.B.) and the NIA (K23 AG046363, EM). This manuscript has been reviewed by DIAN Study investigators for scientific content and consistency of data interpretation with previous DIAN Study publications. We acknowledge the altruism of the participants and their families and contributions of the DIAN research and support staff at each of the participating sites for their contributions to this study. We thank Drs. John Ringman and Bernadino Ghetti for their review and suggestions.

Author Contributions: Sample and data collection involved all authors. Mass Spectrometry analyses was performed by N.R.B. and C.S. Statistical and Imaging analyses were performed by Y.L., C.X., N.J.-M. and B.A.G.. Study design and initial draft of the manuscript was performed by N.R.B., Y.L., R.J.B. and E.M. with significant input on interpretation of the results and additional drafts performed by all coauthors: B.A.G., J.H., T.L.S.B., V.B., A.M.F., R.J.P., A.M.G., J.C.M., C.M.K., C.X., R.A., P.F.C., S.B.B., T.I., H.M., H.S., M.S., K.S., J.N., M.F., J.C., N.R.G.-R., S.S., P.R.S., C.L.M., R.N.M., A.O., N.C.F., J.L., M.J., A.G., S.L.

Competing Interests:

R.J.B. has equity ownership interest in C2N Diagnostics and receive royalty income based on technology (stable isotope labeling kinetics and blood plasma assay) licensed by Washington University to C2N Diagnostics. R.J.B. receives income from C2N Diagnostics for serving on the scientific advisory board. Washington University, with R.J.B. as co-inventor, has submitted the

US nonprovisional patent application “Cerebrospinal fluid (CSF) Tau Rate of Phosphorylation Measurement to Define Stages of Alzheimer’s Disease and Monitor Brain Kinases/Phosphatases Activity." R.J.B. has received honoraria from Janssen and Pfizer as a speaker and from Merck and Pfizer as an Advisory Board member.

E.M. is a co-inventor for US nonprovisional patent application “Cerebrospinal fluid (CSF) Tau Rate of Phosphorylation Measurement to Define Stages of Alzheimer’s Disease and Monitor Brain Kinases/Phosphatases Activity." E.M. has received royalty payments for an educational program supported by Eli Lilly and as member of a Scientific Advisory Board for Eli Lilly.

N.R.B. is a co-inventor for US nonprovisional patent application “Cerebrospinal fluid (CSF) Tau Rate of Phosphorylation Measurement to Define Stages of Alzheimer’s Disease and Monitor Brain Kinases/Phosphatases Activity.

Bibliography

1 Goedert, M., Spillantini, M. G., Jakes, R., Rutherford, D. & Crowther, R. A. Multiple isoforms of human microtubule-associated protein tau: sequences and localization in neurofibrillary tangles of Alzheimer's disease. *Neuron* **3**, 519-526, doi:10.1016/0896-6273(89)90210-9 (1989).

2 Grundke-Iqbal, I. *et al.* Abnormal phosphorylation of the microtubule-associated protein tau (tau) in Alzheimer cytoskeletal pathology. *Proceedings of the National Academy of Sciences of the United States of America* **83**, 4913-4917, doi:10.1073/pnas.83.13.4913 (1986).

3 Kimura, T., Sharma, G., Ishiguro, K. & Hisanaga, S.-i. Phospho-Tau Bar Code: Analysis of Phosphoisotypes of Tau and Its Application to Tauopathy. *Frontiers in Neuroscience* **12**, doi:10.3389/fnins.2018.00044 (2018).

4 Crowther, R. A. Straight and paired helical filaments in Alzheimer disease have a common structural unit. *Proceedings of the National Academy of Sciences* **88**, 2288-2292, doi:10.1073/pnas.88.6.2288 (1991).

5 Fitzpatrick, A. W. P. *et al.* Cryo-EM structures of tau filaments from Alzheimer’s disease. *Nature* **547**, 185, doi:10.1038/nature23002 (2017).

6 Price, J. L., Davis, P. B., Morris, J. C. & White, D. L. The distribution of tangles, plaques and related immunohistochemical markers in healthy aging and Alzheimer's disease. *Neurobiology of aging* **12**, 295-312 (1991).

7 Qian, J., Hyman, B. T. & Betensky, R. A. Neurofibrillary Tangle Stage and the Rate of Progression of Alzheimer Symptoms: Modeling Using an Autopsy Cohort and Application to Clinical Trial Design. *JAMA Neurol* **74**, 540-548, doi:10.1001/jamaneurol.2016.5953 (2017).
8 McDade, E. *et al.* Longitudinal cognitive and biomarker changes in dominantly inherited Alzheimer disease. *Neurology* **91**, e1295-e1306, doi:10.1212/wnl.0000000000006277 (2018).
9 Bateman, R. J. *et al.* Clinical and biomarker changes in dominantly inherited Alzheimer's disease. *The New England journal of medicine* **367**, 795-804, doi:10.1056/NEJMoa1202753 (2012).
10 Fagan, A. M. *et al.* Cerebrospinal fluid tau/beta-amyloid(42) ratio as a prediction of cognitive decline in nondemented older adults. *Arch Neurol* **64**, 343-349, doi:10.1001/archneur.64.3.noc60123 (2007).
11 Vandermeeren, M. *et al.* Detection of tau proteins in normal and Alzheimer's disease cerebrospinal fluid with a sensitive sandwich enzyme-linked immunosorbent assay. *J Neurochem* **61**, 1828-1834 (1993).
12 Mori, H. *et al.* Tau in cerebrospinal fluids: establishment of the sandwich ELISA with antibody specific to the repeat sequence in tau. *Neuroscience Letters* **186**, 181-183, doi:https://doi.org/10.1016/0304-3940(95)11291-4 (1995).
13 Schindler, S. E. *et al.* Emerging cerebrospinal fluid biomarkers in autosomal dominant Alzheimer's disease. *Alzheimer's & Dementia* **15**, 655-665, doi:https://doi.org/10.1016/j.jalz.2018.12.019 (2019).
14 Toledo, J. B., Xie, S. X., Trojanowski, J. Q. & Shaw, L. M. Longitudinal change in CSF Tau and Aβ biomarkers for up to 48 months in ADNI. *Acta Neuropathologica* **126**, 659-670, doi:10.1007/s00401-013-1151-4 (2013).
15 Jack, C. R., Jr. *et al.* NIA-AA Research Framework: Toward a biological definition of Alzheimer's disease. *Alzheimers Dement* **14**, 535-562, doi:10.1016/j.jalz.2018.02.018 (2018).
16 Jack, C. R., Jr. *et al.* A/T/N: An unbiased descriptive classification scheme for Alzheimer disease biomarkers. *Neurology* **87**, 539-547, doi:10.1212/wnl.0000000000002923 (2016).
17 Hu, W. T. *et al.* Reduced CSF p-Tau181 to Tau ratio is a biomarker for FTLD-TDP. *Neurology* **81**, 1945-1952, doi:10.1212/01.wnl.0000436625.63650.27 (2013).
18 Hampel, H. *et al.* Measurement of phosphorylated tau epitopes in the differential diagnosis of Alzheimer disease: a comparative cerebrospinal fluid study. *Archives of general psychiatry* **61**, 95-102, doi:10.1001/archpsyc.61.1.95 (2004).
19 La Joie, R. *et al.* Associations between AV1451 tau PET and CSF measures of tau pathology in a clinical sample. *Neurology* **90**, e282-e290 (2018).
20 Mattsson, N. *et al.* (18)F-AV-1451 and CSF T-tau and P-tau as biomarkers in Alzheimer's disease. *EMBO molecular medicine* **9**, 1212-1223, doi:10.15252/emmm.201707809 (2017).
21 Gordon, B. A. *et al.* Tau PET in autosomal dominant Alzheimer's disease: relationship with cognition, dementia and other biomarkers. *Brain : a journal of neurology* **142**, 1063-1076, doi:10.1093/brain/awz019 (2019).
22 Jack, C. R., Jr *et al.* The bivariate distribution of amyloid-β and tau: relationship with established neurocognitive clinical syndromes. *Brain : a journal of neurology*, doi:10.1093/brain/awz268 (2019).
23 Johnson, K. A. *et al.* Tau positron emission tomographic imaging in aging and early Alzheimer disease. *Annals of neurology* **79**, 110-119, doi:10.1002/ana.24546 (2016).
24 Mattsson, N. *et al.* Predicting diagnosis and cognition with (18)F-AV-1451 tau PET and structural MRI in Alzheimer's disease. *Alzheimers Dement* **15**, 570-580, doi:10.1016/j.jalz.2018.12.001 (2019).

25 Quiroz, Y. T. *et al.* Association Between Amyloid and Tau Accumulation in Young Adults With Autosomal Dominant Alzheimer Disease. *JAMA Neurol* **75**, 548-556, doi:10.1001/jamaneurol.2017.4907 (2018).

26 Bateman, R. J. *et al.* Clinical and biomarker changes in dominantly inherited Alzheimer's disease. *N Engl J Med* **367**, doi:10.1056/NEJMoa1202753 (2012).

27 Fleisher, A. S. *et al.* Associations between biomarkers and age in the presenilin 1 E280A autosomal dominant Alzheimer disease kindred: a cross-sectional study. *JAMA Neurol* **72**, 316-324, doi:10.1001/jamaneurol.2014.3314 (2015).

28 Toledo, J. B., Xie, S. X., Trojanowski, J. Q. & Shaw, L. M. Longitudinal change in CSF Tau and Abeta biomarkers for up to 48 months in ADNI. *Acta Neuropathol* **126**, 659-670, doi:10.1007/s00401-013-1151-4 (2013).

29 Fagan, A. M. *et al.* Longitudinal change in CSF biomarkers in autosomal-dominant Alzheimer's disease. *Sci Transl Med* **6**, 226ra230, doi:10.1126/scitranslmed.3007901 (2014).

30 Price, J. L. & Morris, J. C. Tangles and plaques in nondemented aging and "preclinical" Alzheimer's disease. *Ann Neurol* **45**, 358-368 (1999).

31 Ittner, L. M. *et al.* Dendritic Function of Tau Mediates Amyloid-β Toxicity in Alzheimer's Disease Mouse Models. *Cell* **142**, 387-397, doi:https://doi.org/10.1016/j.cell.2010.06.036 (2010).

32 Cohen, A. D. *et al.* Early striatal amyloid deposition distinguishes Down syndrome and autosomal dominant Alzheimer's disease from late-onset amyloid deposition. *Alzheimer's & dementia : the journal of the Alzheimer's Association*, doi:10.1016/j.jalz.2018.01.002 (2018).

33 Maia, L. F. *et al.* Changes in Amyloid-β and Tau in the Cerebrospinal Fluid of Transgenic Mice Overexpressing Amyloid Precursor Protein. *Science Translational Medicine* **5**, 194re192-194re192 (2013).

34 Sato, C. *et al.* Tau Kinetics in Neurons and the Human Central Nervous System. *Neuron* **98**, 861-864, doi:10.1016/j.neuron.2018.04.035 (2018).

35 Schelle, J. *et al.* Prevention of tau increase in cerebrospinal fluid of APP transgenic mice suggests downstream effect of BACE1 inhibition. *Alzheimer's & Dementia: The Journal of the Alzheimer's Association* **13**, 701-709, doi:10.1016/j.jalz.2016.09.005 (2017).

36 Zempel, H., Thies, E., Mandelkow, E. & Mandelkow, E. M. Abeta oligomers cause localized Ca(2+) elevation, missorting of endogenous Tau into dendrites, Tau phosphorylation, and destruction of microtubules and spines. *J Neurosci* **30**, 11938-11950, doi:10.1523/jneurosci.2357-10.2010 (2010).

37 Saman, S. *et al.* Exosome-associated Tau Is Secreted in Tauopathy Models and Is Selectively Phosphorylated in Cerebrospinal Fluid in Early Alzheimer Disease. *Journal of Biological Chemistry* **287**, 3842-3849, doi:10.1074/jbc.M111.277061 (2012).

38 Jin, M. *et al.* Soluble amyloid β-protein dimers isolated from Alzheimer cortex directly induce Tau hyperphosphorylation and neuritic degeneration. *Proceedings of the National Academy of Sciences* **108**, 5819-5824 (2011).

39 Gordon, B. A. *et al.* Spatial patterns of neuroimaging biomarker change in individuals from families with autosomal dominant Alzheimer's disease: a longitudinal study. *The Lancet. Neurology* **17**, 241-250, doi:10.1016/S1474-4422(18)30028-0 (2018).

40 Ryman, D. C. *et al.* Symptom onset in autosomal dominant Alzheimer disease: a systematic review and meta-analysis. *Neurology* **83**, 253-260, doi:10.1212/WNL.0000000000000596 (2014).

41 Bateman, R. J. *et al.* Clinical and biomarker changes in dominantly inherited Alzheimer's disease. *N Engl J Med* **367**, 795-804, doi:10.1056/NEJMoa1202753 (2012).

42 Morris, J. C. The Clinical Dementia Rating (CDR): current version and scoring rules. *Neurology* **43**, 2412-2414 (1993).

43 Medina, M. & Avila, J. Further understanding of tau phosphorylation: implications for therapy. *Expert review of neurotherapeutics* **15**, 115-122, doi:10.1586/14737175.2015.1000864 (2015).
44 Benzinger, T. L. *et al.* Regional variability of imaging biomarkers in autosomal dominant Alzheimer's disease. *Proc Natl Acad Sci U S A* **110**, E4502-4509, doi:10.1073/pnas.1317918110 (2013).
45 Quiroz, Y. T. *et al.* Cortical atrophy in presymptomatic Alzheimer's disease presenilin 1 mutation carriers. *J Neurol Neurosurg Psychiatry* **84**, 556-561, doi:10.1136/jnnp-2012-303299 (2013).
46 Ridha, B. H. *et al.* Tracking atrophy progression in familial Alzheimer's disease: a serial MRI study. *Lancet Neurol* **5**, 828-834, doi:10.1016/s1474-4422(06)70550-6 (2006).
47 Arriagada, P. V., Growdon, J. H., Hedley-Whyte, E. T. & Hyman, B. T. Neurofibrillary tangles but not senile plaques parallel duration and severity of Alzheimer's disease. *Neurology* **42**, 631-631, doi:10.1212/wnl.42.3.631 (1992).
48 Okonkwo, O. C. *et al.* Cerebrospinal fluid profiles and prospective course and outcome in patients with amnestic mild cognitive impairment. *Archives of neurology* **68**, 113-119, doi:10.1001/archneurol.2010.334 (2011).
49 Bateman, R. J. *et al.* The DIAN-TU Next Generation Alzheimer's prevention trial: Adaptive design and disease progression model. *Alzheimers Dement* **13**, 8-19, doi:10.1016/j.jalz.2016.07.005 (2017).
50 Yanamandra, K. *et al.* Anti-tau antibody administration increases plasma tau in transgenic mice and patients with tauopathy. *Science Translational Medicine* **9**, eaal2029, doi:10.1126/scitranslmed.aal2029 (2017).
51 He, Z. *et al.* Amyloid-beta plaques enhance Alzheimer's brain tau-seeded pathologies by facilitating neuritic plaque tau aggregation. *Nat Med* **24**, 29-38, doi:10.1038/nm.4443 (2018).
52 Buerger, K. *et al.* CSF phosphorylated tau protein correlates with neocortical neurofibrillary pathology in Alzheimer's disease. *Brain : a journal of neurology* **129**, 3035-3041, doi:10.1093/brain/awl269 (2006).
53 Ittner, A. *et al.* Site-specific phosphorylation of tau inhibits amyloid-β toxicity in Alzheimer's mice. *Science* **354**, 904-908 (2016).
54 Potter, R. *et al.* Increased in Vivo Amyloid-β42 Production, Exchange, and Loss in Presenilin Mutation Carriers. *Science Translational Medicine* **5**, 189ra177-189ra177 (2013).
55 Yamada, K. *et al.* In Vivo Microdialysis Reveals Age-Dependent Decrease of Brain Interstitial Fluid Tau Levels in P301S Human Tau Transgenic Mice. *The Journal of Neuroscience* **31**, 13110-13117, doi:10.1523/jneurosci.2569-11.2011 (2011).
56 van der Kant, R. *et al.* Cholesterol Metabolism Is a Druggable Axis that Independently Regulates Tau and Amyloid-β in iPSC-Derived Alzheimer's Disease Neurons. *Cell Stem Cell* **24**, 363-375.e369, doi:https://doi.org/10.1016/j.stem.2018.12.013 (2019).

Figure Legends:

Figure 1. Stages of tau pathology: tau pathophysiology evolves through distinct phases in dominantly inherited Alzheimer's disease. Measuring four different soluble tau species and

aggregated tau in dominantly inherited Alzheimer's disease we show over the course of 35 years tau sequentially changes by stage of disease related to amyloid plaques, cortical atrophy and metabolism. **A**. Starting with the development of fibrillar amyloid pathology, tau phosphorylation at position 217 (purple) and 181 (blue) begins to increase. **B**. With the increase in neuronal dysfunction (decreased cortical metabolism), phosphorylation at position 205 (green) begins to increase along with soluble total tau (orange). **C**. Lastly, with the onset of neurodegeneration (based on cortical atrophy and clinical decline) tau PET tangles (red) begin to develop while phosphorylation of 217 and 181 decreases. Together, the dynamic and diverging patterns of soluble and aggregated tau change over the course of the disease and begin in close relationship with amyloid pathology.

Figure 2. Longitudinal changes of different phosphorylated-tau sites are stage of disease specific and change in opposite directions as AD progresses in dominantly inherited mutation carriers.

Linear mixed effect model estimated annual rates of change for each site of phosphorylation based on the standardized MC data (n=370) and plotted over EYO along with PiB-PET (black, n=304) and cognitive decline (aqua, n=356); the solid circles represent the point when the rate of change for each variable first becomes different for mutation carriers compared to non-carriers. This highlights the pattern of change for p-tau isoforms over the course of the AD spectrum and the close association between amyloid plaque growth and the increase in pT217/T217 with plaques beginning to increase at -21 EYO and the hyperphosphorylation of pT217 (purple) also beginning at -21, followed by pT181 (blue) increase in hyperphosphorylation at -19 EYO and the phosphorylation rate declining in these two sites associated with a decline in cognition. In contrast, phosphorylation of pT205 (green) continues increasing throughout disease progression

and total tau levels (orange) increase at an increased rate near the time of symptom onset. However, phosphorylation of pS202 does not increase throughout the disease course.

Figure 3. Specific soluble tau phosphorylation sites are differentially associated with amyloid plaques in dominantly inherited and sporadic AD. a. Receiver operating characteristics of tau phosphorylation with Aß pathology based on Aβ PiB-PET (SUVR cutoff of 1.25) in DIAD (n=252), demonstrates a near perfect association with Aβ pathology for pT217/T217 (purple, AUC=0.97), with different associations with pT181/T181 (blue, AUC =0.89), pT205/T205 (green, AUC = 0.74), total tau (orange, AUC=0.72) and pS202/S202 (gray, AUC=0.69). **b1-5.** Standardized (z-score) phosphorylation ratios **pT217/T217, pT181/T181, pS202/S202**, **pT205/T205** and **total tau** levels by Aβ PiB-PET quartiles (n=47 Q1, n=48 Q2, n=48 Q3, n=48 Q4) for mutation carriers suggests site-specific differences in phosphorylation with increasing. Aβ PiB-PET levels: p-T217, p-T181, p-T205 and total tau increase as Aβ PiB-PET increases. For pS202/S202, there was a significant decrease in phosphorylation at the highest Aβ PiB-PET quartiles relative to the lowest; based on Wilcoxon rank sum test; the middle line represents the median, and the upper and lower notch = median +/- 1.58 * interquartile range/ square root(n-observations), the upper and lower whisker = largest observation greater/less than or equal to upper/lower hinge + 1.58 * IQR. **c1-5**. Change in phosphorylation rate and total tau levels for DIAD (n=209) and sAD (n=86) across the spectrum of clinical progression (blue = cognitively normal/ amyloid negative). For DIAD there is evidence of a higher ratio of phosphorylation and in both DIAD and sAD, phosphorylation of pT217 and pT181 increases once amyloid pathology begins, followed by a plateau. In contrast, pT205 and total tau levels increase at later stages of disease progression. For pS202 in both DIAD and sAD, there is minimal change in phosphorylation rate across the disease spectrum;

based on Mann-Whitney U test; the middle line represents the median, and the upper and lower notch = median +/- 1.58 * interquartile range/ square root(n-observations), the upper and lower whisker = largest observation greater/less than or equal to upper/lower hinge + 1.58 * IQR. **d.** Cross-sectional, bivariate correlations between cortical and sub-cortical Aβ PiB-PET SUVR and site-specific phosphorylation for asymptomatic mutation carriers (n=152). The colors represent the correlation with positive correlations (yellow-red) and negative correlations (blue). P values for the correlations are derived from z test using the covariance matrix of the bivariate linear mixed effects models. All correlations represent statistically significant values surviving a false discovery rate ($p < 0.05$) using Benjamini Hochberg method and are arranged by the strength of the correlations from top to bottom.

Figure 4. Tau phosphorylation positions are differentially related to brain atrophy and hypometabolism in dominantly inherited AD.

a. Bivariate correlations between cortical and sub-cortical atrophy and site-specific phosphorylation ratios in asymptomatic mutation carriers (n= 152) demonstrates increases in phosphorylation of pT205/T205 and pT217/T217, followed by t-tau and less for pT181/T181.**b**. Bivariate correlations between cortical and sub-cortical brain metabolism measured by FDG-PET and site-specific phosphorylation ratios in asymptomatic mutation carriers (n= 152) demonstrates an increase in phosphorylation of pT205/T205 is associated with a decrease in most cortical and sub-cortical regions but not for other p-tau sites or total tau. P values for the correlations were calculated using Chi-square tests based on the bivariate linear mixed effects models with Benjamini Hochberg method for correction of multiple comparison.

Figure 5. In dominantly inherited AD, elevated levels of tau phosphorylation decline in some sites with onset of dementia in contrast to a continued rise in total tau. .

Individual estimated annualized rates of change of p-tau isoforms and total tau, standardized for all mutation carriers, (y-axis) for mutation carriers were correlated with the annualized change in global cognitive function (**a-d**); the lines represent simple linear regression with shaded area representing 95% confidence interval. Each point is an individual level correlation between measures, with the Pearson's r for all data. The linear regression was fit to those with no dementia (CDR 0, black triangle, n= 49) and dementia (CDR >0, red circle, n= 27). A decline in pT217/T217 (a), r= 0.71($p < 0.0001$), pT181/T181 (b), r= 0.79 ($p < 0.0001$) and pT205/T205, r= 0.21($p=0.06$) phosphorylation rate was associated with cognitive decline after symptom onset (red). For total tau there was an inverse correlation with cognition (d), r= -0.79($p < 0.0001$). (**e**) A linear fit for all mutation carriers demonstrates there are distinct associations between declining cognition and changes in the different p-tau isoforms and total tau: with decreases in pT217/T217 and pT181/T181 and an increase in total tau associated with cognitive decline; and no associations with pT205/T205 or pS202/S202. This suggests that soluble tau species are not equivalent in AD (pS202/S202 is shown here to demonstrate the lack of association with cognition, r= -0.09 ($p=0.39$)). Statistical significance for all the correlations was based on two-sided t test.

Table 1. Demographic, cerebrospinal fluid, neuroimaging and cognition measures for mutation carriers (MC), non-carriers (NC) and non-familial at risk and symptomatic cohort. Continuous measures are presented as the mean ± standard deviation. For MC and NC, the significance of difference among asymptomatic MC, symptomatic MC and NC was calculated using *t* test based on linear (for continuous outcome) and generalized linear with a logistic link (for

categorical outcome) mixed effects models. All the mixed models included a random family effect to account for the correlations on the outcome measures between participants within the same family. For non-familial at risk and symptomatic cohort, the p-values were calculated from a one-way ANOVA (for continuous outcome) and Chi-square test (for categorical outcome).

		Mutation Carriers		Mutation non-carriers	p-value
	(Asymptomatic MC/Symptomatic MC/ NC) N	Asymptomatic (N = 152)	Symptomatic (N = 77)	(N = 141)	
Age	370	34.4 ± 8.9	46.2 ± 9.2	38.5 ± 12.2	<.0001
Female, n (%)	370	84 (55.3)	39 (50.7)	88 (62.4)	0.15
APOE ε4, n (%)	370	48 (31.6)	23 (29.9)	51 (36.2)	0.67
EYO	370	-13.4 ± 8.7	3.42 ± 3.47	-9.2 ± 12.5	<.0001
Cortical PiB PET SUVR	304 (133/50/121)	1.76 ± 0.89	2.82 ± 1.27	1.06 ± 0.17	<.0001
***PiB +, n (%)**	304 (133/50/121)	81 (60.9)	48 (96.0)	2 (1.65)	<.0001
CSF pT181/T181 (phospho/unphospho)	370	26.5 ± 7.2	34.2 ± 7.7	21.7 ± 2.3	<.0001
CSF pT181 level (ng/ml)	370	0.14 ± 0.09	0.30 ± 0.19	0.088 ± 0.034	<.0001
CSF pT205/T205 (phospho/unphospho)	370	0.44 ± 0.24	0.93 ± 0.36	0.34 ± 0.13	<.0001
CSF pT205 level (ng/ml)	370	0.003 ± 0.003	0.011 ± 0.008	0.002 ± 0.001	<.0001
CSF pT217/T217 (phospho/unphospho)	370	3.49 ± 3.08	8.42 ± 4.05	1.25 ± 0.66	<.0001
CSF pT217 level (ng/ml)	370	0.015 ± 0.018	0.054 ± 0.047	0.004 ± 0.004	<.0001
CSF pS202/S202 (phospho/unphospho)	370	2.77 ± 0.80	2.52 ± 0.68	3.10 ± 0.72	<.0001
CSF pS202 level (ng/ml)	370	0.016 ± 0.006	0.025 ± 0.011	0.014 ± 0.005	<.0001
CSF tau level (ng/ml)	370	0.51 ± 0.21	0.82 ± 0.41	0.40 ± 0.14	<.0001

Precuneus (mm)	344 (146/64/134)	2.37 ± 0.15	2.10 ± 0.24	2.38 ± 0.14	<.0001
Cortical FDG PET SURV	318 (137/59/122)	1.73 ± 0.14	1.57 ± 0.18	1.71 ± 0.14	<.0001
Hippocampal volume (mm^3)	344 (146/64/134)	8863 ± 970	7290 ± 1214	8787 ± 775	<.0001
Cognitive Composite (z-score)	356 (151/66/139)	-0.096 ± 0.640	-1.67 ± 0.85	-0.03 ± 0.59	<.0001
At risk and sporadic AD cohort					
	(amyloid negative/ asymptomatic/ symptomatic) N	Amyloid negative (N = 39)	Amyloid positive		
			Asymptomatic (N=18)	Symptomatic (N = 45)	F- value
Age	102	73.3 ± 8.6	71.6 ± 6.4	72.6 ± 6.2	0.41
Female, n (%)	102	17(44)	8(44)	31(69)	0.041(p-value)
MMSE	102	28.7 ± 1.6	29.4 ± 0.5	23.6 ± 3.9	45.44***
CSF pT181/T181 (phospho/unphospho)	102	13.8 ± 1.3	16.6 ± 2.9	18.8 ± 2.5	53.55***
CSF pT205/T205 (phospho/unphospho)	102	0.14 ± 0.06	0.2 ± 0.08	0.33 ± 0.11	50.6***
CSF pT217/T217 (phospho/unphospho)	102	3.3 ± 1.4	8.2 ± 4.8	10 ± 4.1	39.18***
CSF pS202/S202 (phospho/unphospho)	102	1.4 ± 0.48	1.2 ± 0.33	1.38 ± 0.45	1.042
CSF tau level (ng/ml)	102	0.76 ± 0.31	0.89 ± 0.32	1.1 ± 0.41	7.14**

EYO- estimated years to onset of symptoms; PiB- Pittsburgh compound B; p-phosphorylated; S- serine; SUVR- standard uptake value ratio; T- threonine. PiB + = SUVR >1.25. Significance **codes** for F-value: **'***' 0.001 '**' 0.01 '*' 0.05**, else > 0.05.

Methods:

Study Design

Participants

Participants with at least 50% risk of inheriting an DIAD mutation from families with a confirmed genetic mutation in *PSEN1, PSEN2 or APP* were enrolled in the Dominantly Inherited Alzheimer Network study (DIAN, NIA U19 AG032438) (dian.wustl.edu; clinicaltrials.gov number NCT00869817)[57]. All procedures were approved by the Institutional Review Board (IRB) of Washington University and conformed to local IRB and Ethics Committees where the study was being performed. The presence or absence of a DIAD mutation was determined using PCR-based amplification of the appropriate exon followed by Sanger sequencing. At each study visit, participants underwent comprehensive clinical assessments, cognitive testing, neuroimaging, and CSF studies; however, at each visit, each participant may not have completed all study procedures. The details of study structure and assessments can be found in prior publications [41,57]. Follow-up intervals were determined by clinical status (normal or impaired) of each participant and by their estimated years to symptom onset (EYO) and ranged from yearly to every three years. Data was obtained from quality-controlled data (yearly quality assessments for irregular results and missing data from January 26, 2009 to June 30, 2017) and included 370 participants (n=150 with longitudinal CSF evaluations with a median time between visits of 2.8 years).

The non-familial population represented two cohorts recruited at the Knight Alzheimer Disease Research Center at Washington University and the Centre Mémoire Resources Recherche,

Centre Hospitalier Universitaire (CHU) Montpellier. All participants underwent detailed clinical cognitive assessments, cerebrospinal fluid assessments and a diagnosis of preclinical AD or AD confirmed with abnormal amyloid biomarkers. All procedures were approved by the IRB of Washington University and Ethics Committees at CHU Montpellier.

Estimated Years to Symptom Onset (EYO)

In dominantly inherited AD there is near 100% penetrance, with age at symptom onset in mutation carriers being relatively consistent for each mutation and within each family. This allows for the designation of estimated years to symptom onset (EYO). EYO was defined as follows: A *parental* age at earliest symptom onset was established for each participant by semi-structured interview. The parental age at onset for each mutation was then entered into a database consisting of the combined symptom onset values from DIAN and from prior publications from DIAD cohorts. These were used to compute an average age of onset specific to each mutation[40]. The mutation-specific age of onset was subtracted from each participant's age at the time of clinical assessment to define the individual's EYO. When a specific mutation average age of onset was unknown, the parental or proxy age of onset was used to define EYO[40]. For participants who were symptomatic at baseline, as assessed by a CDR >0, the reported age of actual symptom onset was subtracted from age at each clinical assessment to define EYO.

Clinical Assessments

Standardized clinical evaluations, including the use of a study partner, were performed for each DIAD participant. The Clinical Dementia Rating Scale (CDR) was used to indicate dementia stage. Participants were rated as cognitively normal (CDR=0) or having very mild dementia (CDR= 0·5), mild dementia (CDR= 1) or moderate dementia (CDR =2)[42]. Evaluating clinicians

were blind to genetic status. A comprehensive neuropsychological battery assessing general cognitive function, memory, attention, executive function, visuospatial function, and language was performed at each visit[58]. From these tests we developed a cognitive composite that reliably detects decline across the range of EYO and CDR[59]. The composite represents the average of the z scores from tests including *episodic memory, complex attention, and processing speed* and a *general cognitive screen* (Mini-Mental State Examination).

For the non-familial cohorts, all participants underwent a standardized, detailed clinical assessment specific to each of the two centers. A diagnosis of AD was based on the National Institute of Neurological and Communicative Disorders and Stroke- Alzheimer Disease and Related Disorders Association (NINCDS-ADRDA)[60] criteria and confirmed with abnormal amyloid biomarkers. Dementia severity was based on CDR. Additional details of the cohort can be found in previous publications[61].

CSF Tau Analyses

CSF was collected via standard lumbar puncture procedures using an atraumatic Sprotte spinal needle (22Ga) into two 13ml polypropylene tubes. CSF was flash-frozen upright on dry ice. Samples collected in the United States were shipped overnight on dry ice to the DIAN Biomarker Core laboratory at Washington University, St. Louis, MO, USA, whereas samples collected at international sites were stored at -80°C and shipped quarterly on dry-ice. Upon arrival, each sample was subsequently thawed, combined into a single polypropylene tube, and aliquoted (500µl each) into polypropylene microcentrifuge tubes (#05-538-69C, Corning Life Science, Corning, NY, USA), after which they were re-flash frozen on dry-ice and stored at −80°C.

814 Each thawed CSF sample was mixed with 25µl of a solution containing 15N-441 tau internal
815 standard (2.5ng per sample), 50mM Guanidine, 10% NP-40 and 10X protease inhibitor cocktail
816 (Roche, Basel, Switzerland). Tau was extracted by immune capture using incubation under
817 rotation at room temperature during 2 hours with 20µl of sepharose beads cross-linked to Tau1
818 (tau epitope 192-199) and HJ8.5 (tau epitope 27-35) antibodies. Beads were spun by
819 centrifugation, then rinsed three times with 1ml of 25mM TEABC. Samples were digested
820 overnight at 37°C with 400 ng of trypsin Gold (Promega, Madison, WI). AQUA peptides (Life
821 Technologies, Carlsbad, CA) were spiked to obtain an amount of 5fmol per labeled
822 phosphorylated peptide and 50fmol per labeled unmodified peptide in each sample. The peptide
823 mixture was loaded on TopTip C18 tips, washed with 0.1% Formic Acid (FA) solution and
824 eluted with 60% ACN 0.1% FA solution. Eluates were dried using a Speedvac and dried samples
825 were stored at -80°C prior to analysis. Samples were resuspended in 25µl of 2% ACN 0.1% FA.
826 Extracts were analyzed by nanoLC-MS/HRMS using Parallel Reaction Monitoring using HCD
827 fragmentation. NanoLC-MS/MS experiments were performed using a nanoAcquity UPLC
828 system (Waters, Mildford, MA) coupled to a Fusion Tribrid mass spectrometer (Thermo
829 Scientific, San Jose, CA). 5µl was injected for each sample. Peptide separation was achieved at
830 60°C in 24 minutes on a Waters HSS T3 column (75µm x 100mm, 1.8µm). Mobile phases were
831 (A) 0.1% formic acid in water and (B) 0.1% formic acid in acetonitrile. Gradient used
832 was: 0min-0.5% B; 7.5min-5% B; 22min-18% B; then the column was rinsed 2 minutes with
833 95% B. Flow rate was set at 700nl/min for 7.5min then 400nl/min for the rest of the analysis.
834 Data were acquired in the positive ion mode at a spray voltage of 2200V (Nanospray Flex Ion
835 Source, Thermo Scientific) and ion transfer tube set at 270°C. S-lens RF voltage was set at 60 V.
836 MS/HRMS transitions (Supplemental Table 14) and were extracted using Skyline software

(MacCoss lab, University of Washington). CSF tau phosphorylation levels were calculated using measured ratios between MS/HRMS transitions of endogenous unphosphorylated peptides and 15N labeled peptides from protein internal standard. Ratio of phosphorylation on T181, S202, T205 and T217 were measured using the ratio of the MS/HRMS transitions from phosphorylated peptides and corresponding unphosphorylated peptides. Each phosphorylated/unphosphorylated peptide endogenous ratio was normalized using the ratio measured on the MS/HRMS transitions of the corresponding AQUA phosphorylated/unphosphorylated peptide internal standards.

All samples from the DIAN longitudinal and the cross sectional studies were run together with waste CSF (longitudinal and cross sectional study) and CSF pool (cross sectional) QC controls to monitor inter-assay variability for each variables at low CSF tau (normal level) and high CSF tau (AD typical level) levels. Corresponding values and inter-assay coefficient of variation (CV) have been incorporated in supplemental tables. In both studies, inter-assay CV were typically below 20%. A low percentage of the investigated samples had CSF pT205 and pT217 levels below the lowest limit of quantitation (4.7 and 4.5% respectively), defined as levels providing LC-MS signals leading to more than 20% of CV.

CSF samples from sporadic AD at WU were collected as described previously[61]. Aliquots from the collection performed at hour 32 were used for the analysis. CSF samples from sporadic AD at Montpellier were collected in polypropylene tubes using lumbar puncture methods (Starstedt; 10mL, ref 62.610.201) in line with standard operating procedures[62], transferred at a temperature of 4◦C within less than 4h to the laboratory and centrifuged at1000g at 4◦C for 10min. 0.5-mLaliquots of CSF supernatant were subsequently collected in 1.5-mL Eppendorf microtubes (Eppendorf Protein LoBind, ref0030108.116) and stored at –80◦C before shipping on dry ice, additional storage at -80◦C and analysis. These samples were used/tested without performing an

additional freeze-thaw cycle. The methods used for the handling/traceability of the samples were in keeping with the procedures recommended in the biobank quality standard NFS 96–900, for which the laboratory is certified. Additional details were described previously[63].

Brain Imaging

Amyloid deposition, glucose metabolism, tau (NFT) PET and cortical thickness/subcortical volumes were assessed using ^{11}C-PiB-PET, ^{18}F-FDG-PET, ^{18}F-AV-1451 (a.k.a flortaucipir) and volumetric T1-weighted MRI scans, respectively. Standard procedures were used to ensure consistency in the data collection of all DIAN sites[39]. The ^{11}C-PiB-PET scan consisted of 70 minutes of dynamic scanning after a bolus injection of ~13 mCi of PiB with regional standard uptake ratios (SUVR) determined from the 40-70-minute timeframe. The ^{18}F-FDG-PET scan started 30 minutes after a ~5 mCi bolus injection and lasted 30 minutes. The ^{18}F-AV-1451 data was acquired from the 80-100-minute window after bolus injection and were converted to SUVRs. The T1 MR sequence was an accelerated magnetization-prepared rapid acquisition with gradient echo (MPRAGE) acquired on 3T scanners (parameters: TR=23000, TE=2.95, and $1.0\times1.0\times1.2mm^3$ resolution). All tau and PiB-PET data have previously been reported in previous publications[8,21].

The PIB and FDG SUVRs from 34 cortical and 6 subcortical regions of interests (ROIs) were obtained using FreeSurfer software (http://surfer.nmr.mgh.harvard.edu/). The SUVRs were processed with total cerebellum grey matter as reference regions and ROI data were corrected for partial volume effects using a regional point spread function (RSF)[64] in geometric transfer matrix framework.

Statistical analysis

Baseline characteristics of the participants were summarized as mean ± SD for continuous variables and n (column percent) for categorical variables. P-values for comparing the differences among asymptomatic MC, symptomatic MC and NC as defined at baseline were obtained using linear mixed effects models (LME) for continuous variables and generalized LME, with a logistic link for categorical variables. All of the models incorporated a random family effect to account for the correlations on the outcome measures between participants within the same family. The cut point for baseline cortical PiB PET SUVR was chosen such that the difference in the longitudinal rate of change of cortical PiB PET between MC and NC first starts to differ significantly different from 0.

The cross-sectional relationship of the different tau phosphorylation sites with PiB, FDG, and Cortical thickness/Subcortical volume were evaluated in all asymptomatic MCs (CDR=0, n=152) using multivariate LME on each ROI. The models included fixed effects of EYO and random intercepts at the family level. Compared with the simple correlation estimation method (Pearson or Spearman correlation), the multivariate LME can adjust for covariates such as EYO as well as accounting for the correlation within the family cluster[65,66]. P-values for testing the correlations were corrected using the Benjamini Hochberg method[67] to control the false discovery rate due to multiple testing.

For within-individual annual rate of change over the longitudinal follow up, the best linear unbiased predictors for each biomarker were estimated using LME, which were then plotted against baseline EYO to examine biomarkers trajectories. Linear or linear spline mixed effects models, where appropriate, were then used to determine the baseline EYO point from which MC became significantly different from NC in baseline level and the rate of change for each biomarker. The details of the linear spline mixed effects models can be found in a recent

905 publication[8]. The linear or linear spline mixed effects models included the fixed effects of
906 mutation group (MC or NC), baseline EYO, time since baseline and all possible two-way or
907 three-way interactions among them. Sex, years of education, and *APOE ε4* status were
908 considered as covariates, but only those effects that were significant were retained in the models.
909 Random effects included in the models were the random intercepts for family clusters, individual
910 random intercept and random slope with unstructured covariance matrix to account for the
911 within-subject correlation due to repeated measures. The adjusted difference in the mean level at
912 baseline and difference in the rates of change between MC and NC were then tested using the
913 approximate *t*-test derived from the models to determine the first EYO point where the difference
914 became significant.

915 To visualize the differences in the rates of change among total tau, tau phosphorylation site,
916 cortical PiB, and global cognition across the range of EYO, measures of MC were first
917 standardized using the mean and standard deviation of the NC. The rate of change of each
918 measure for each MC were then calculated using LME, and LOESS curves were fitted to visually
919 represent the trajectories of the standardized rates of change over EYO.

920 The utility of baseline and annual rate of change of total tau and p-tau in predicting longitudinal
921 cognitive decline among MC were evaluated using LME controlling for the effect of baseline
922 age, sex and APOE ε4 status. Random effects in the models included the random intercepts for
923 family clusters, individual random intercept and random slope with unstructured covariance
924 matrix.

925 Linear regressions were used to examine whether the annual rate of change of tau and phospho-
926 tau position for MC and NC, leading up to and including the point when the tau PET was

performed, could predict tau PET SUVR, controlling for the effect of age. Due to the limited number of participants, a family cluster was not included.

All analyses were conducted using SAS 9.4 (SAS Institute Inc., Cary, NC) and RStudio (version 3.4.3). A p-value <0.05 was considered to be statistically significant and all statistical tests were two-sided.

Data availability

The data that support the findings of this study can be requested from DIAN at https://dian.wustl.edu/our-research/observational-study/dian-observational-study-investigator-resources/.

Code availability

All codes used for data analyses are available upon request to the corresponding authors.

Bibliography

8 McDade, E. *et al.* Longitudinal cognitive and biomarker changes in dominantly inherited Alzheimer disease. *Neurology* **91**, e1295-e1306, doi:10.1212/wnl.0000000000006277 (2018).

21 Gordon, B. A. *et al.* Tau PET in autosomal dominant Alzheimer's disease: relationship with cognition, dementia and other biomarkers. *Brain : a journal of neurology* **142**, 1063-1076, doi:10.1093/brain/awz019 (2019).

39 Gordon, B. A. *et al.* Spatial patterns of neuroimaging biomarker change in individuals from families with autosomal dominant Alzheimer's disease: a longitudinal study. *The Lancet. Neurology* **17**, 241-250, doi:10.1016/S1474-4422(18)30028-0 (2018).

40 Ryman, D. C. *et al.* Symptom onset in autosomal dominant Alzheimer disease: a systematic review and meta-analysis. *Neurology* **83**, 253-260, doi:10.1212/WNL.0000000000000596 (2014).

41 Bateman, R. J. *et al.* Clinical and biomarker changes in dominantly inherited Alzheimer's disease. *N Engl J Med* **367**, 795-804, doi:10.1056/NEJMoa1202753 (2012).

42 Morris, J. C. The Clinical Dementia Rating (CDR): current version and scoring rules. *Neurology* **43**, 2412-2414 (1993).

57 Morris, J. C. *et al.* Developing an international network for Alzheimer research: The Dominantly Inherited Alzheimer Network. *Clin Investig (Lond)* **2**, 975-984, doi:10.4155/cli.12.93 (2012).

58 Storandt, M., Balota, D. A., Aschenbrenner, A. J. & Morris, J. C. Clinical and psychological characteristics of the initial cohort of the Dominantly Inherited Alzheimer Network (DIAN). *Neuropsychology* **28**, 19-29, doi:10.1037/neu0000030 (2014).

59 Lim, Y. Y. *et al.* BDNF Val66Met moderates memory impairment, hippocampal function and tau in preclinical autosomal dominant Alzheimer's disease. *Brain* **139**, 2766-2777, doi:10.1093/brain/aww200 (2016).

60 McKhann, G. *et al.* Clinical diagnosis of Alzheimer's disease: report of the NINCDS-ADRDA Work Group under the auspices of Department of Health and Human Services Task Force on Alzheimer's Disease. *Neurology* **34**, 939-944, doi:10.1212/wnl.34.7.939 (1984).

61 Patterson, B. W. *et al.* Age and amyloid effects on human central nervous system amyloid-beta kinetics. *Annals of neurology* **78**, 439-453, doi:10.1002/ana.24454 (2015).

62 del Campo, M. *et al.* Recommendations to standardize preanalytical confounding factors in Alzheimer's and Parkinson's disease cerebrospinal fluid biomarkers: an update. *Biomark Med* **6**, 419-430, doi:10.2217/bmm.12.46 (2012).

63 Barthelemy, N. R. *et al.* Tau Protein Quantification in Human Cerebrospinal Fluid by Targeted Mass Spectrometry at High Sequence Coverage Provides Insights into Its Primary Structure Heterogeneity. *Journal of proteome research* **15**, 667-676, doi:10.1021/acs.jproteome.5b01001 (2016).

64 Su, Y. *et al.* Partial volume correction in quantitative amyloid imaging. *Neuroimage* **107**, 55-64, doi:10.1016/j.neuroimage.2014.11.058 (2015).

65 Luo, J., D'Angelo, G., Gao, F., Ding, J. & Xiong, C. Bivariate correlation coefficients in family-type clustered studies. *Biometrical Journal* **57**, 1084-1109, doi:doi:10.1002/bimj.201400131 (2015).

66 Xiong, C. *et al.* Longitudinal relationships among biomarkers for Alzheimer disease in the Adult Children Study. *Neurology* **86**, 1499-1506, doi:10.1212/WNL.0000000000002593 (2016).

67 Benjamini, Y., and Hochberg, Y. . Controlling the false discovery rate: a practical and powerful approach to multiple testing. *Journal of the Royal Statistical Society* **Series B**, 289-300 (1995).

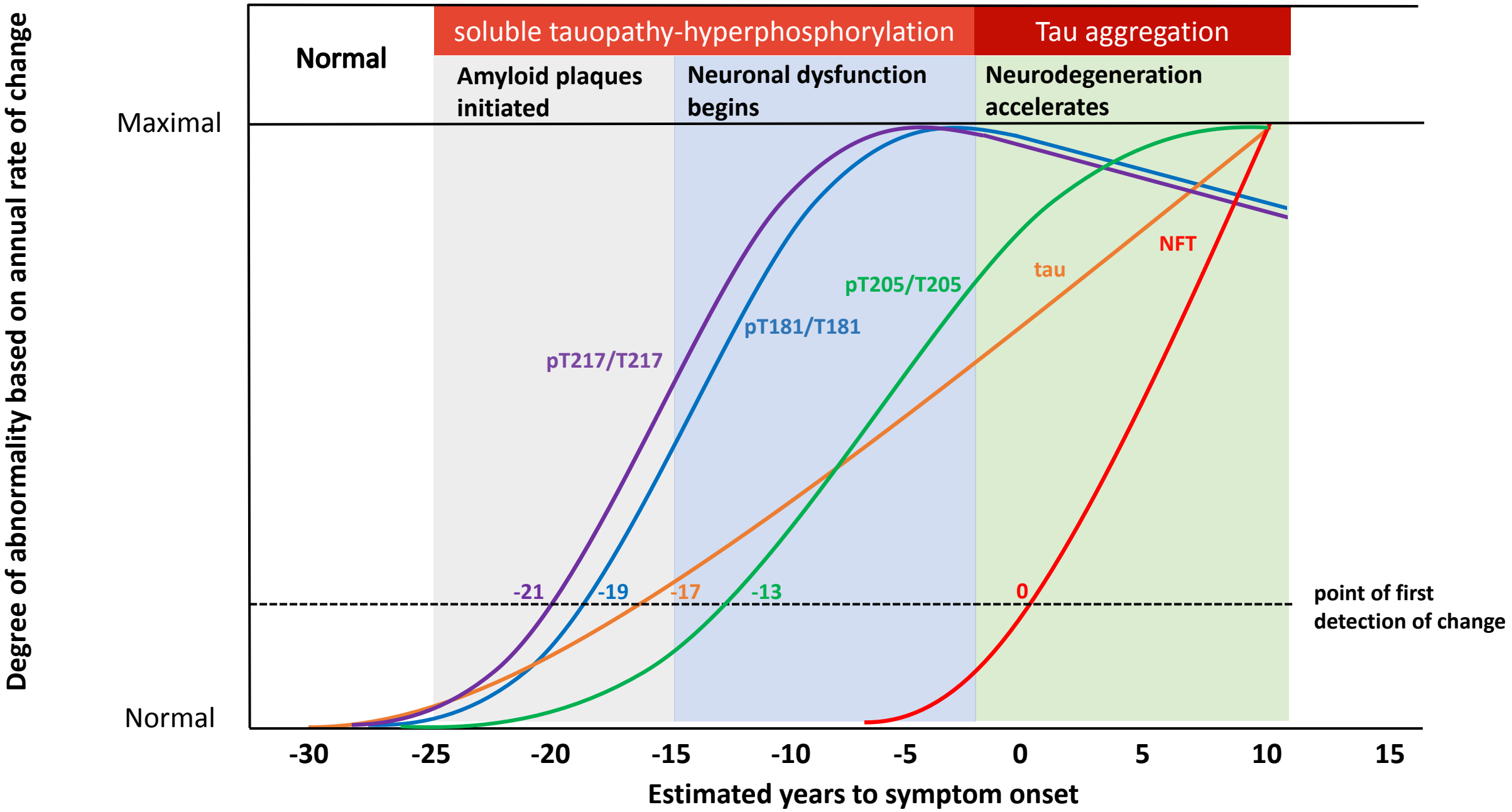
Degree of abnormality based on annual rate of change
Maximal
Normal
Normal
soluble tauopathy-hyperphosphorylation
Tau aggregation
Amyloid plaques initiated
Neuronal dysfunction begins
Neurodegeneration accelerates
pT217/T217
pT181/T181
pT205/T205
tau
NFT
-21
-19
-17
-13
0
point of first detection of change
-30
-25
-20
-15
-10
-5
0
5
10
15
Estimated years to symptom onset

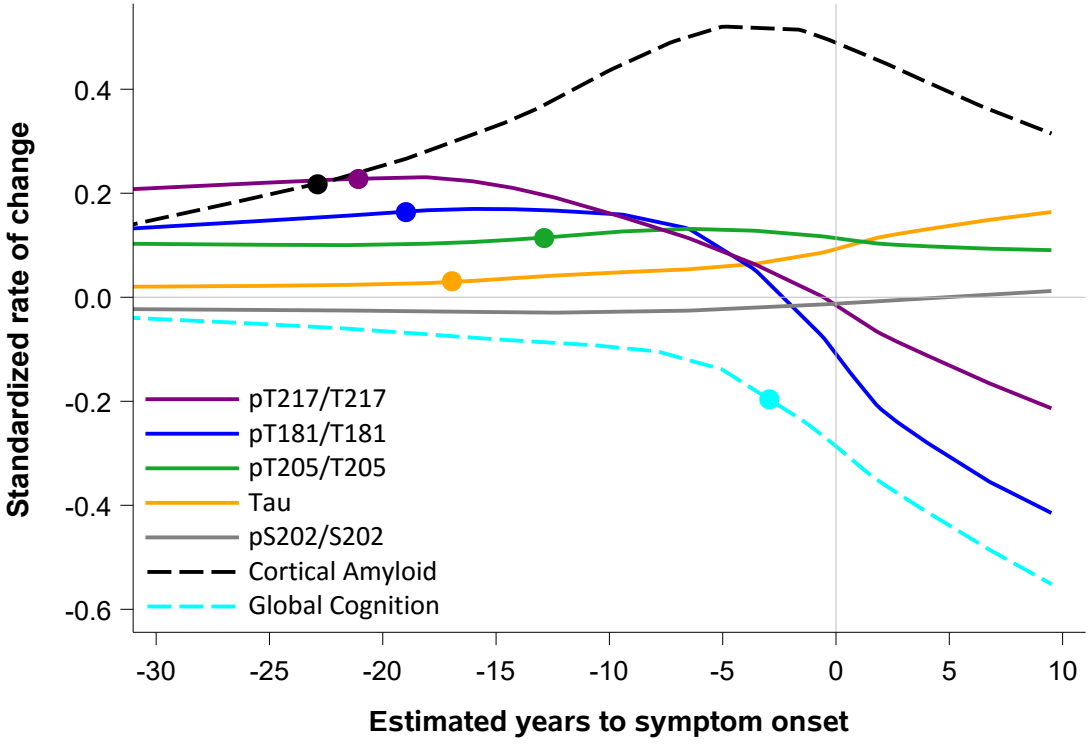
Standardized rate of change
0.4
0.2
0.0
-0.2
-0.4
-0.6
pT217/T217
pT181/T181
pT205/T205
Tau
pS202/S202
Cortical Amyloid
Global Cognition
-30
-25
-20
-15
-10
-5
0
5
10
Estimated years to symptom onset

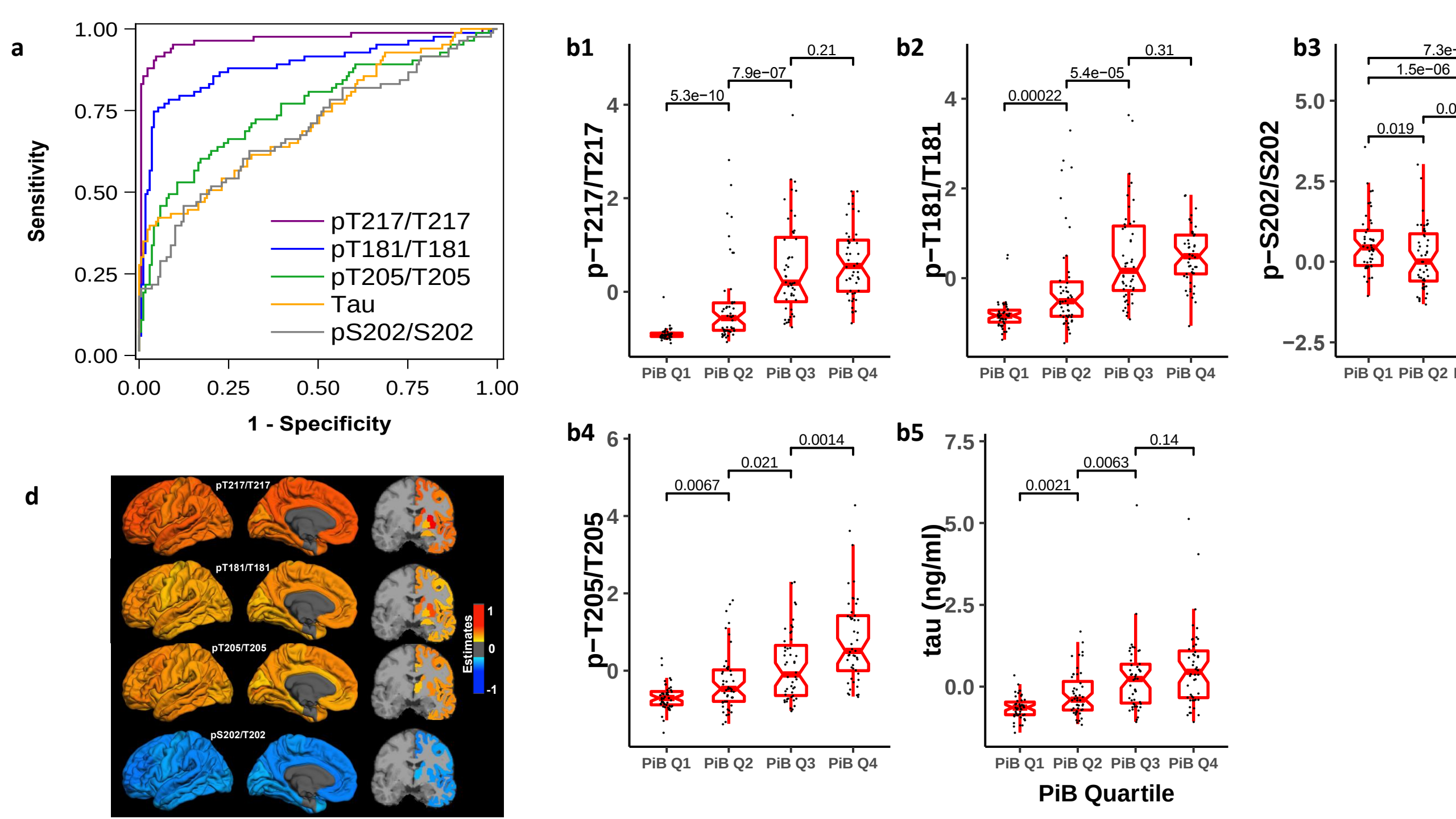
a
Sensitivity
1 - Specificity
0.00
0.25
0.50
0.75
1.00
pT217/T217
pT181/T181
pT205/T205
Tau
pS202/S202
b1
p−T217/T217
5.3e−10
7.9e−07
0.21
b2
p−T181/T181
0.00022
5.4e−05
0.31
b3
p−S202/S202
0.019
b4
p−T205/T205
0.0067
0.021
0.0014
b5
tau (ng/ml)
0.0021
0.0063
0.14
PiB Q1
PiB Q2
PiB Q3
PiB Q4
PiB Quartile
d
pT217/T217
pT181/T181
pT205/T205
pS202/T202
Estimates
1
0
-1

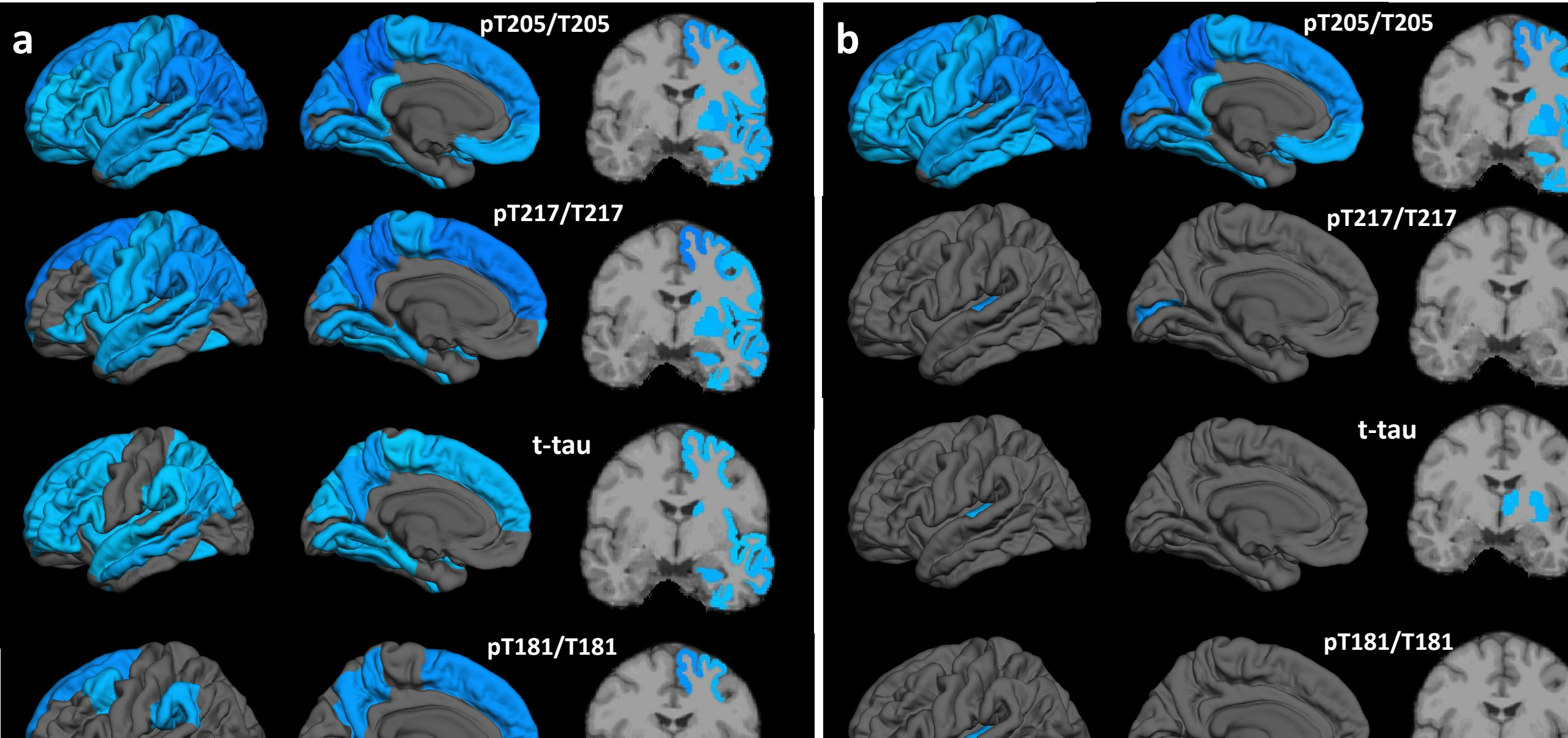
Brain Thickness
Brain Metabolism
a
b
pT205/T205
pT217/T217
t-tau
pT181/T181
pT205/T205
pT217/T217
t-tau
pT181/T181

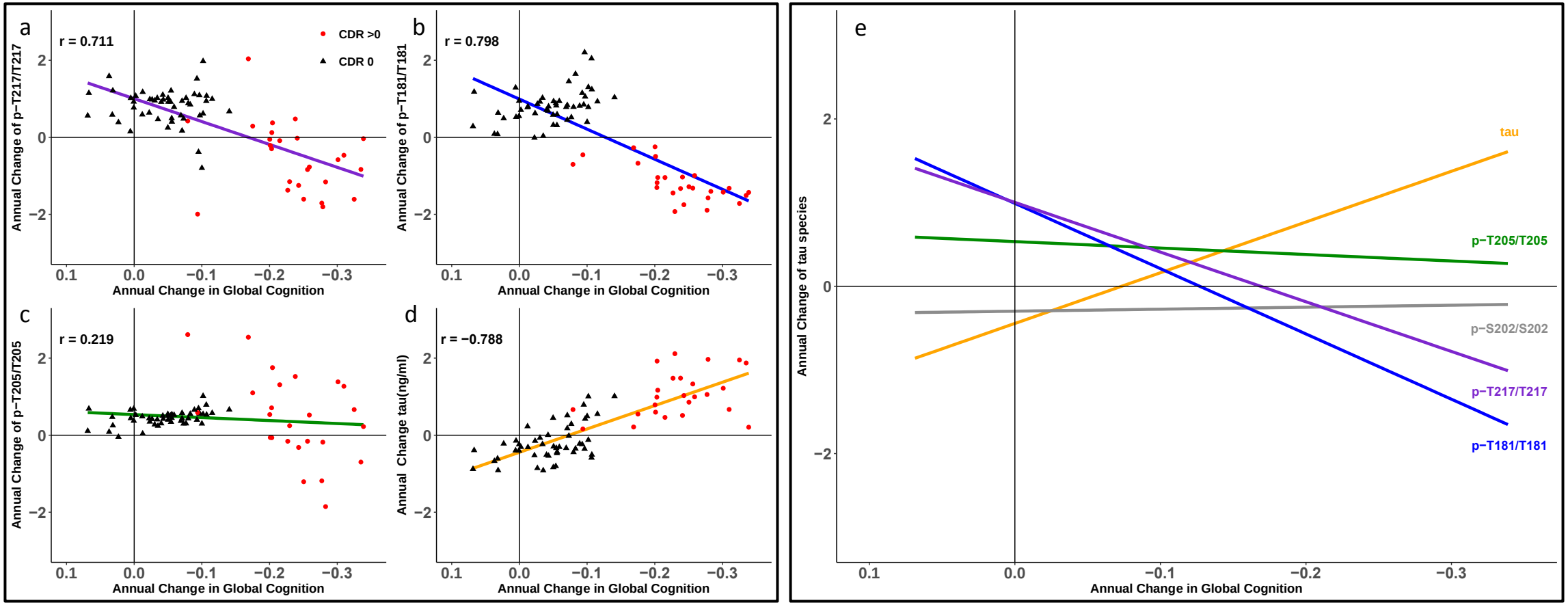
a
r = 0.711
CDR >0
CDR 0
Annual Change of p−T217/T217
Annual Change in Global Cognition
b
r = 0.798
Annual Change of p−T181/T181
Annual Change in Global Cognition
c
r = 0.219
Annual Change of p−T205/T205
Annual Change in Global Cognition
d
r = −0.788
Annual Change tau(ng/ml)
Annual Change in Global Cognition
e
Annual Change of tau species
tau
p−T205/T205
p−S202/S202
p−T217/T217
p−T181/T181
Annual Change in Global Cognition

a

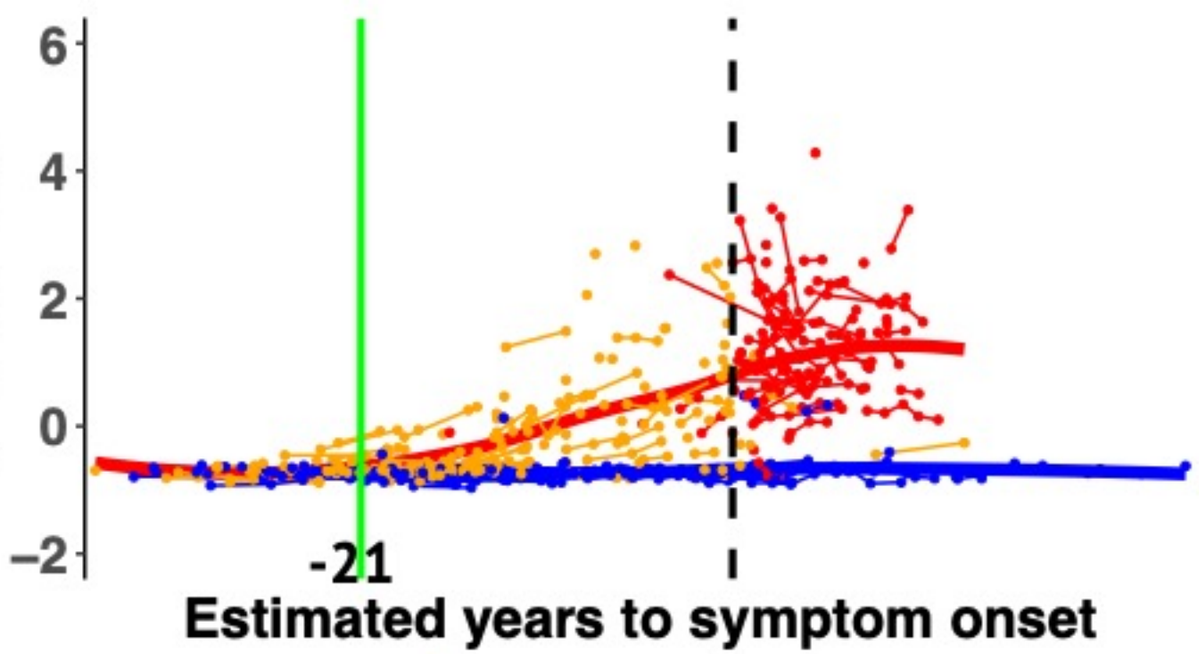
p−T217/T217
6
4
2
0
−2
-21
Estimated years to symptom onset

b

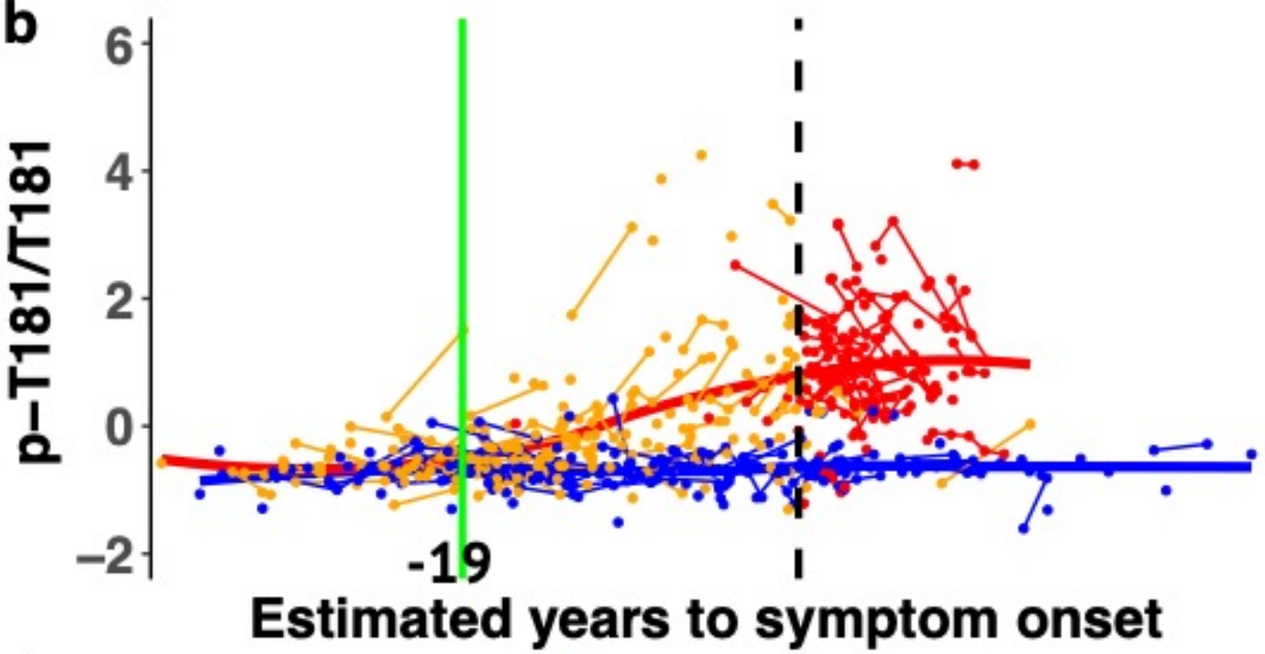
p−T181/T181
6
4
2
0
−2
-19
Estimated years to symptom onset

c

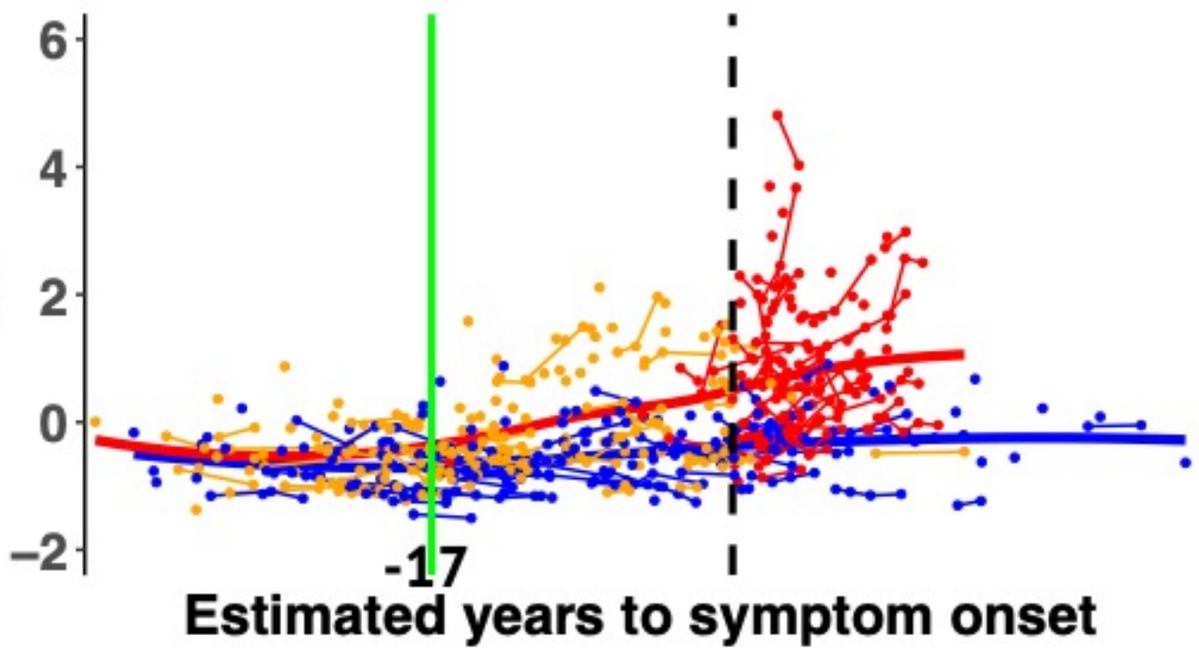
Tau
6
4
2
0
−2
-17
Estimated years to symptom onset

d

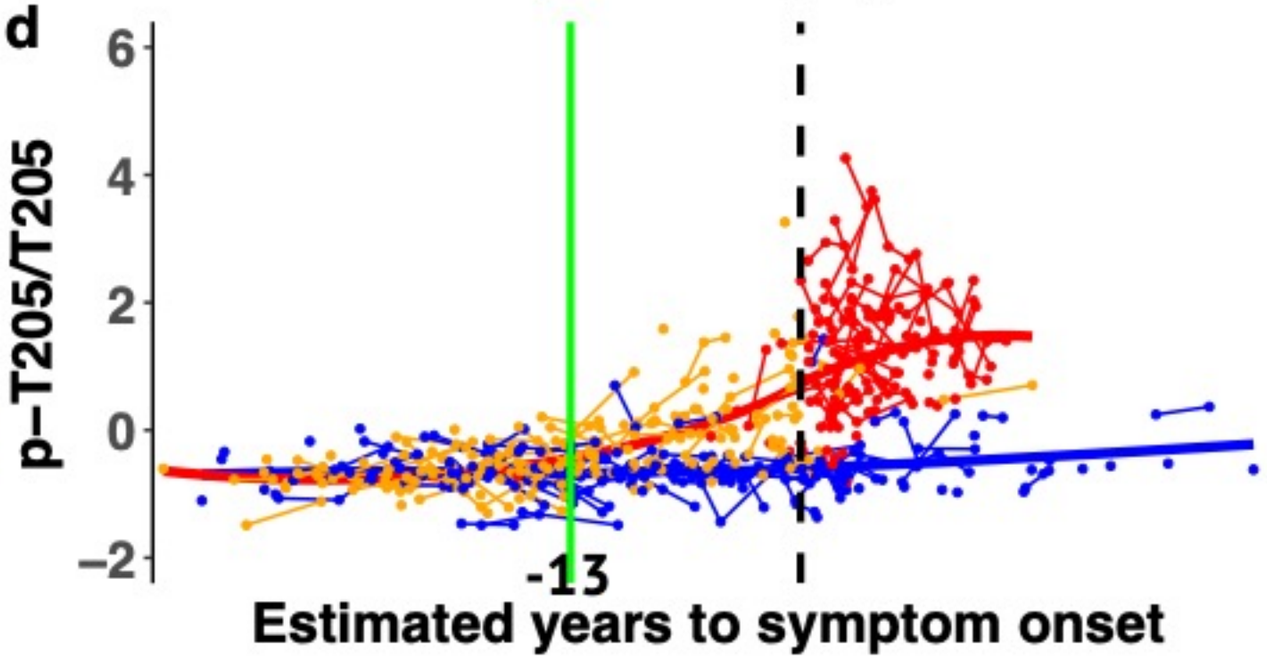
p−T205/T205
6
4
2
0
−2
-13
Estimated years to symptom onset

e

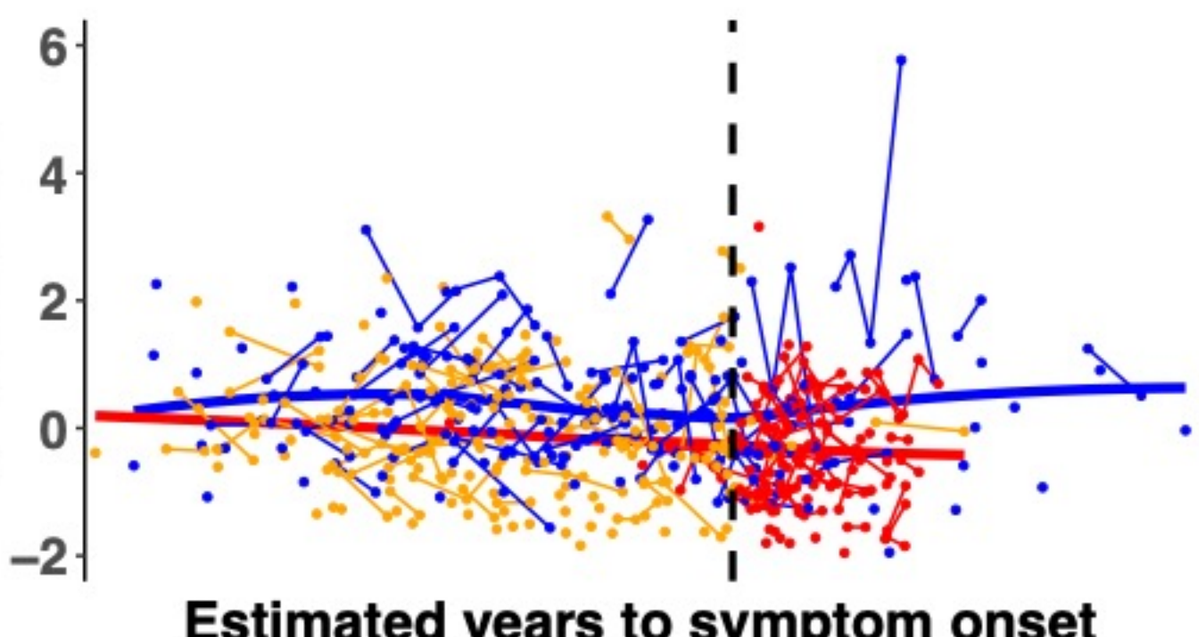
p−S202/S202
6
4
2
0
−2
Estimated years to symptom onset

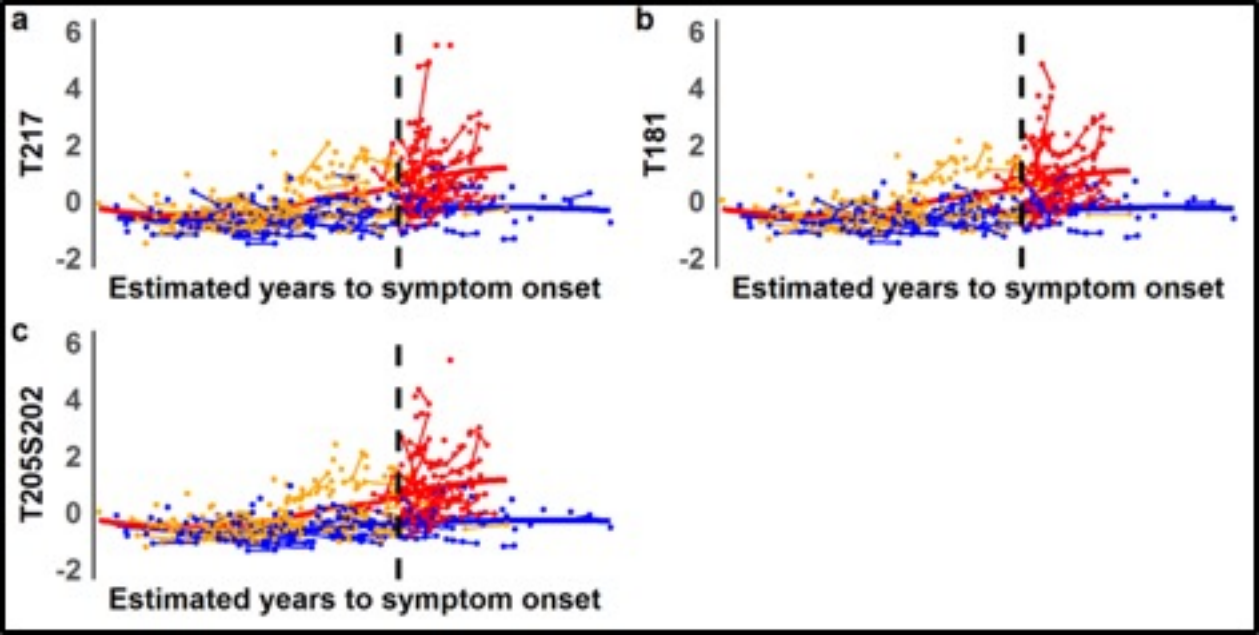
a
T217
6
4
2
0
-2
Estimated years to symptom onset
b
T181
6
4
2
0
-2
Estimated years to symptom onset
c
T205S202
6
4
2
0
-2
Estimated years to symptom onset

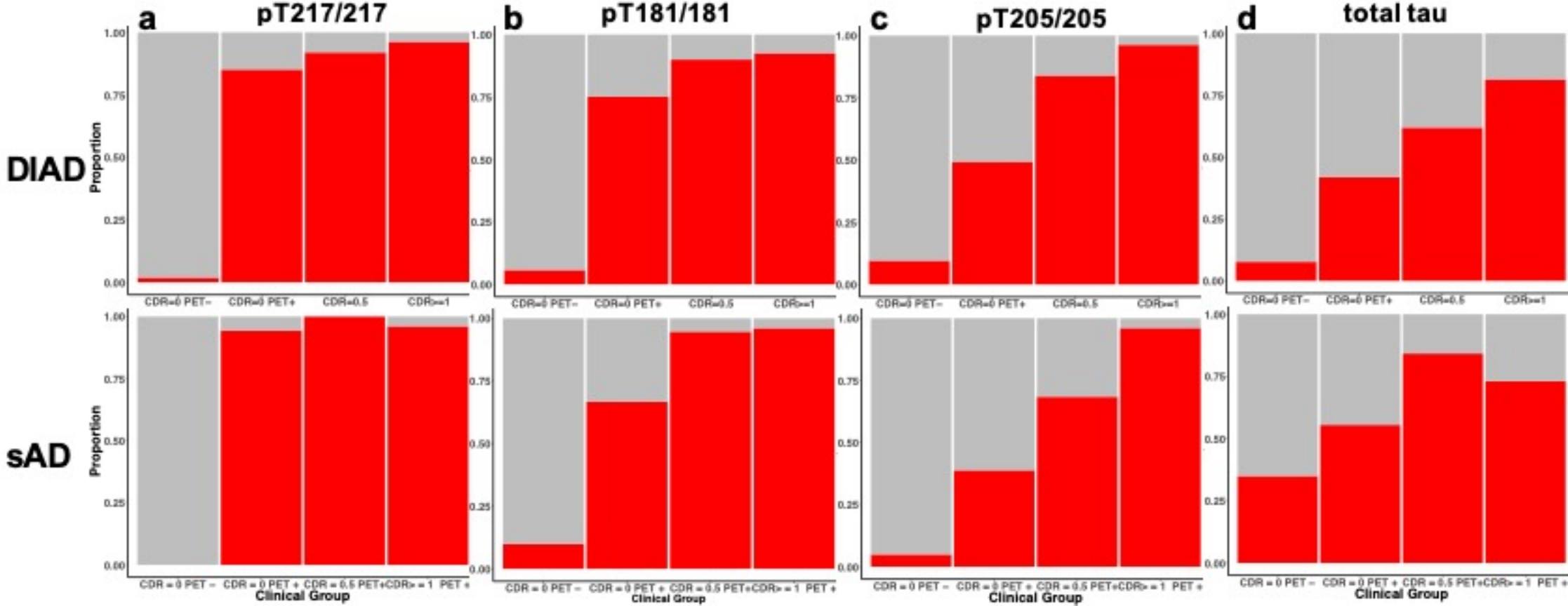
a
pT217/217
b
pT181/181
c
pT205/205
d
total tau
DIAD
sAD
Proportion
1.00
0.75
0.50
0.25
0.00
CDR=0 PET−
CDR=0 PET+
CDR=0.5
CDR>=1
CDR = 0 PET −
CDR = 0 PET +
CDR = 0.5 PET+
CDR>= 1 PET +
Clinical Group

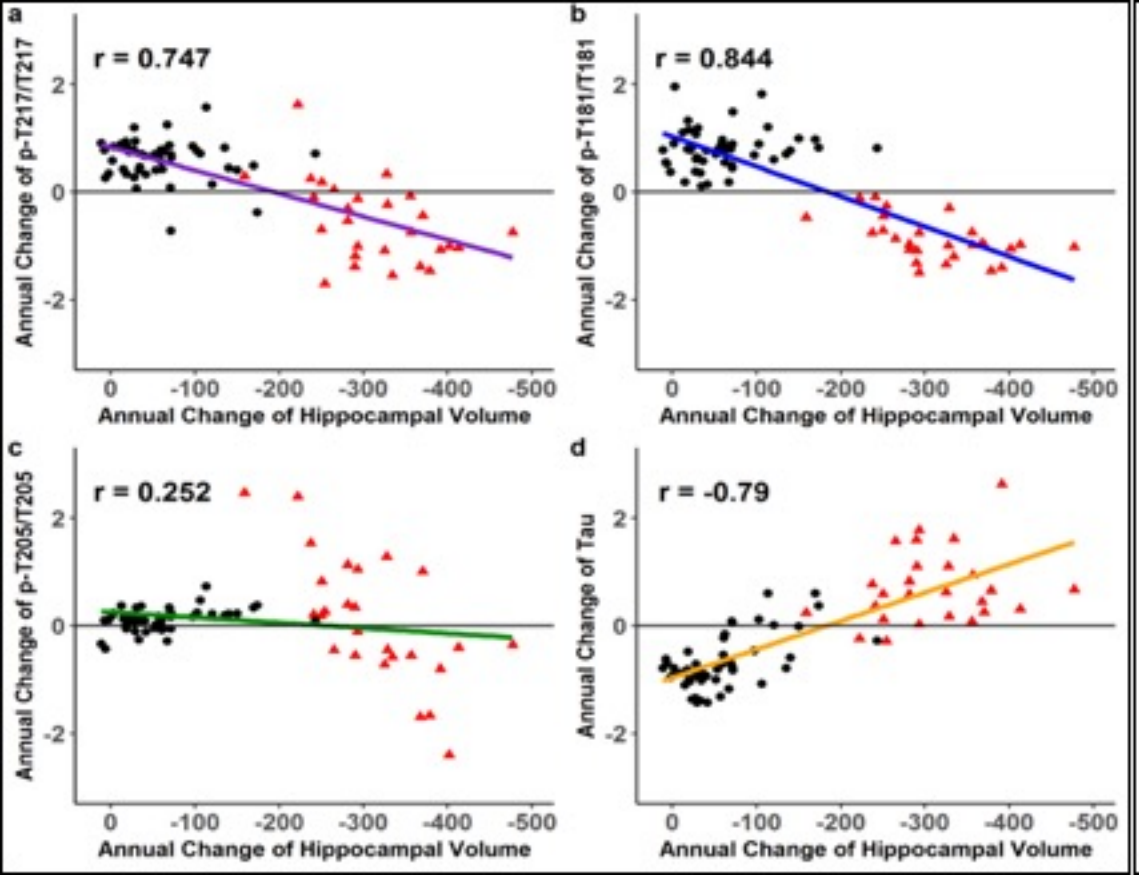
a
r = 0.747
Annual Change of p-T217/T217
Annual Change of Hippocampal Volume
b
r = 0.844
Annual Change of p-T181/T181
Annual Change of Hippocampal Volume
c
r = 0.252
Annual Change of p-T205/T205
Annual Change of Hippocampal Volume
d
r = -0.79
Annual Change of Tau
Annual Change of Hippocampal Volume
2
0
-2
0
-100
-200
-300
-400
-500

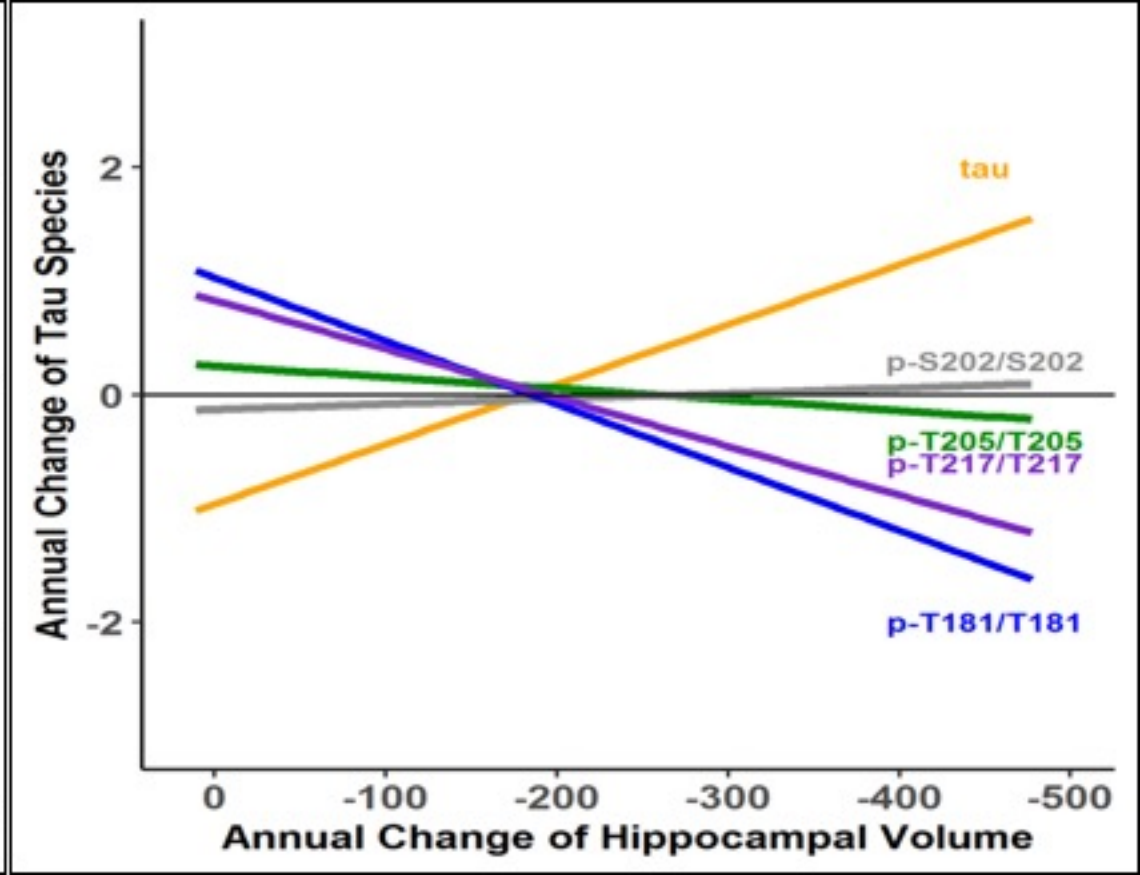
Annual Change of Tau Species
Annual Change of Hippocampal Volume
tau
p-S202/S202
p-T205/T205
p-T217/T217
p-T181/T181
2
0
-2
0
-100
-200
-300
-400
-500

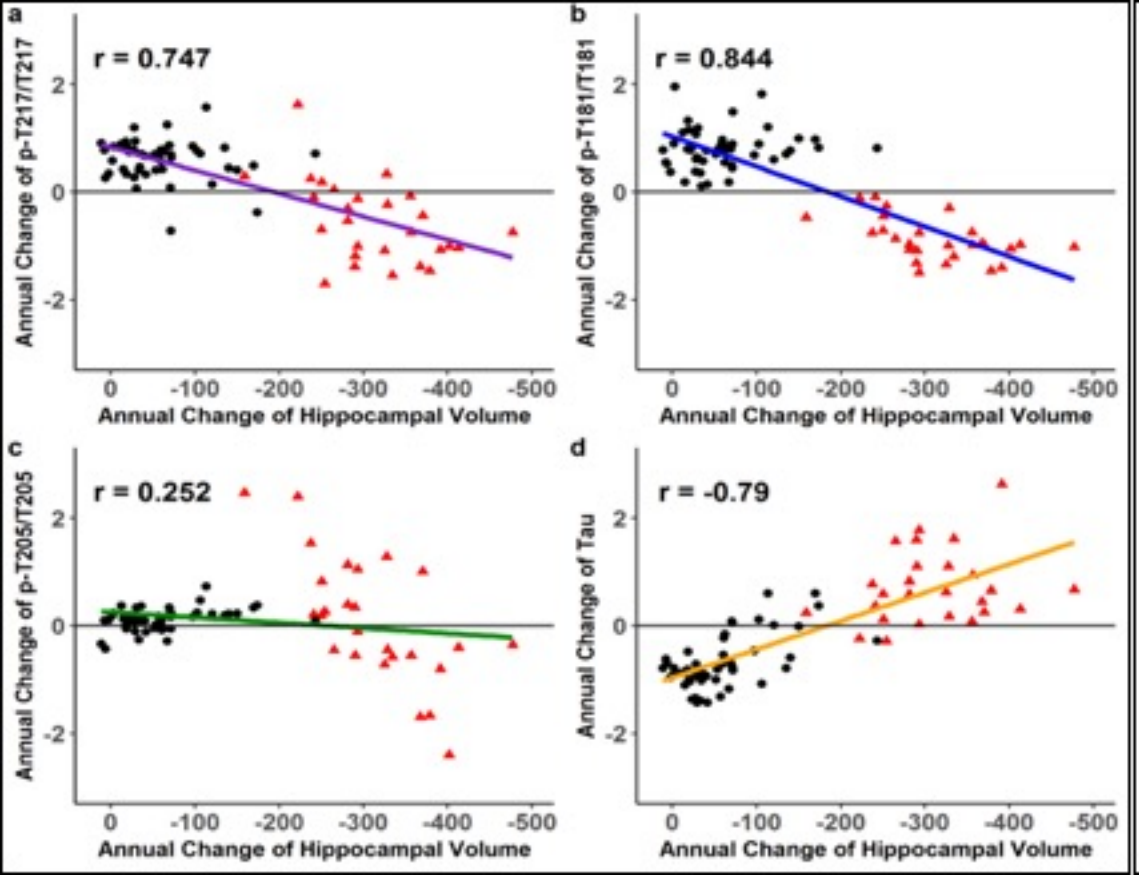
a
r = 0.747
Annual Change of p-T217/T217
Annual Change of Hippocampal Volume
b
r = 0.844
Annual Change of p-T181/T181
Annual Change of Hippocampal Volume
c
r = 0.252
Annual Change of p-T205/T205
Annual Change of Hippocampal Volume
d
r = -0.79
Annual Change of Tau
Annual Change of Hippocampal Volume
2
0
-2
0
-100
-200
-300
-400
-500

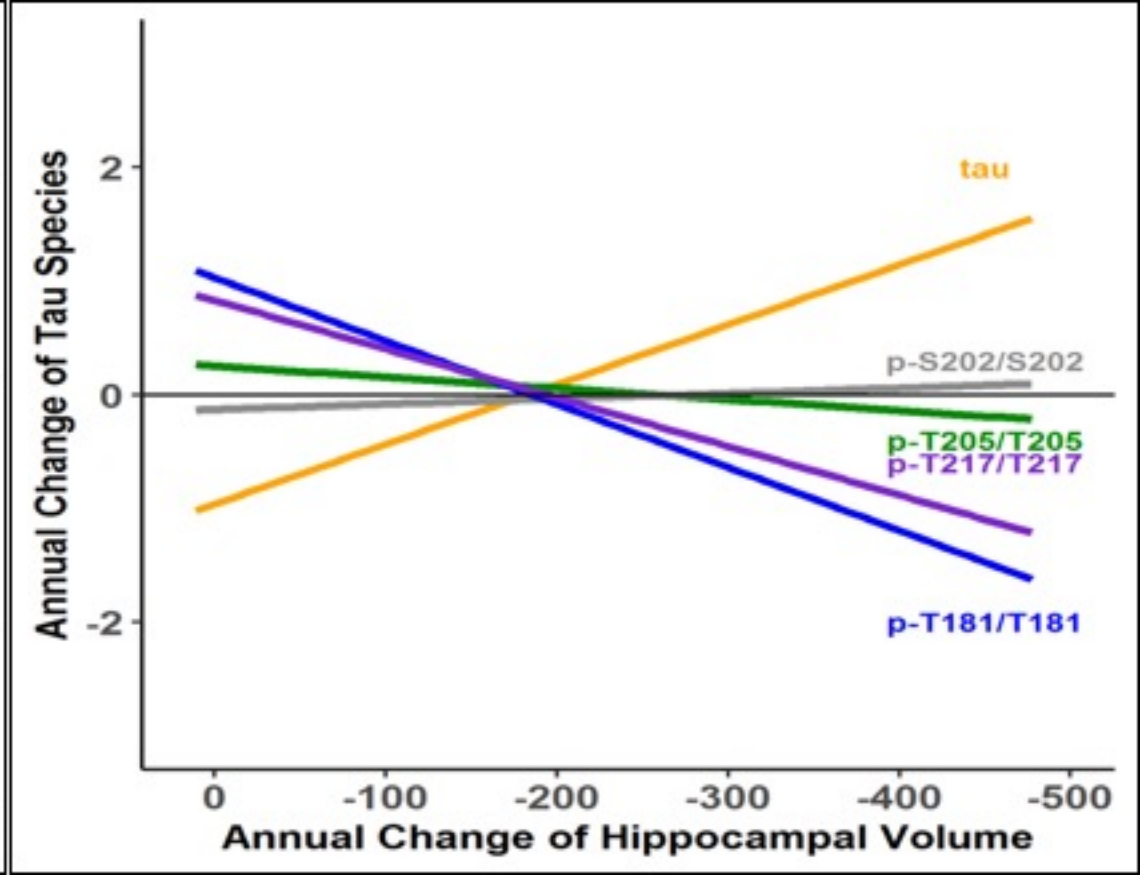
Annual Change of Tau Species
Annual Change of Hippocampal Volume
tau
p-S202/S202
p-T205/T205
p-T217/T217
p-T181/T181
2
0
-2
0
-100
-200
-300
-400
-500

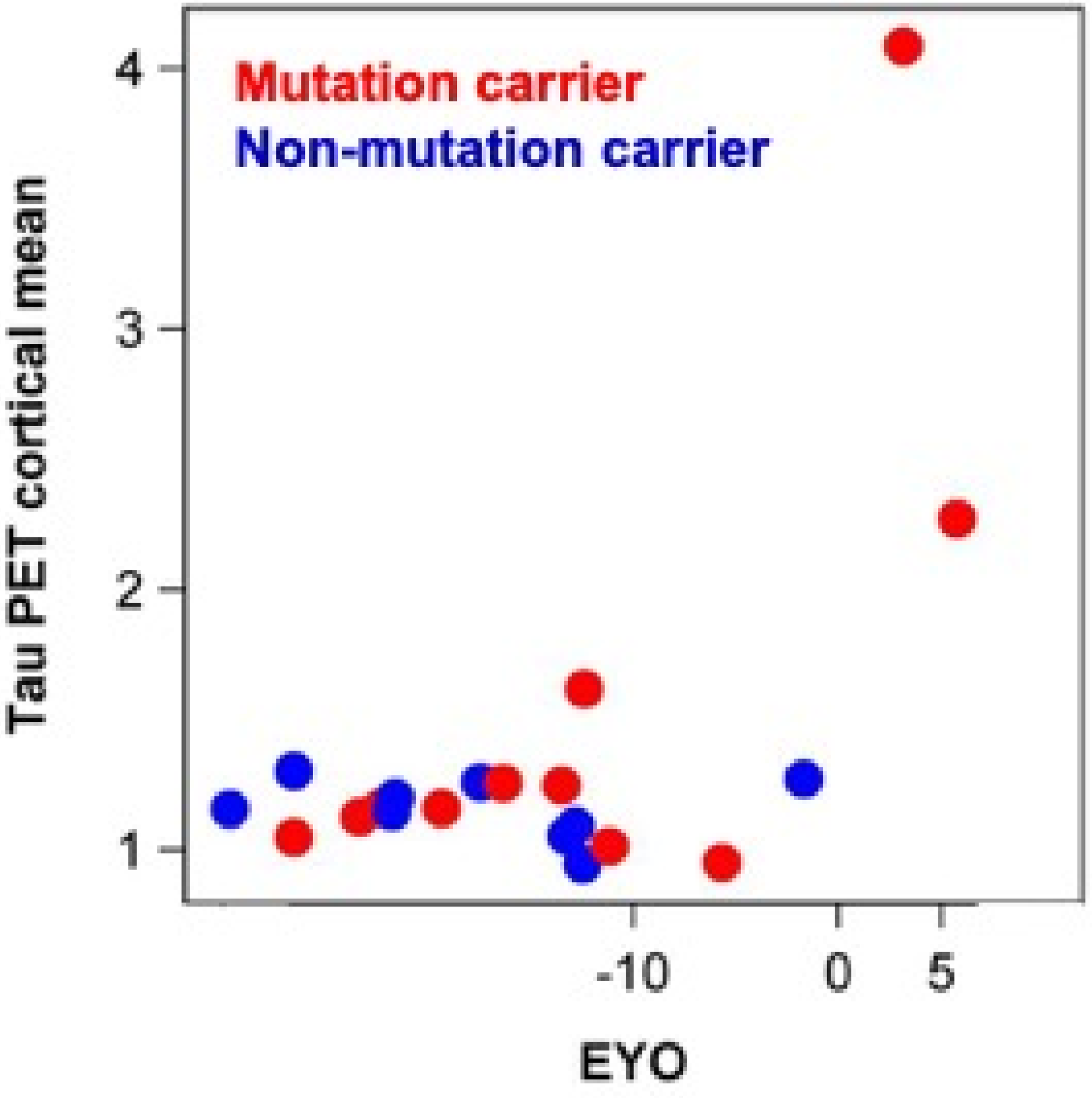
Mutation carrier
Non-mutation carrier
Tau PET cortical mean
4
3
2
1
-10
0
5
EYO

a
b
c
d
e
Tau PET cortical mean
Tau PET cortical mean
Tau PET cortical mean
Tau PET cortical mean
Tau PET cortical mean

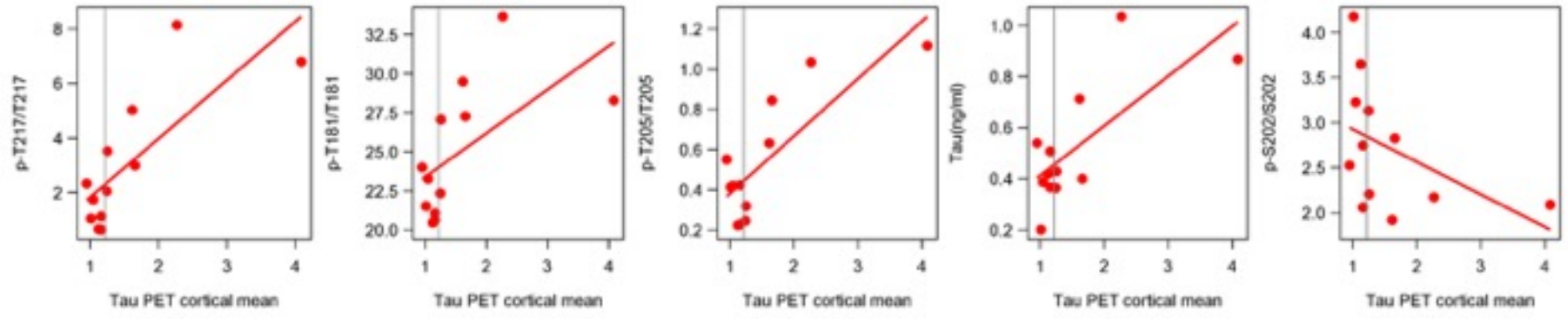
p-T217/T217
p-T181/T181
p-T205/T205
Tau(ng/ml)
p-S202/S202
Tau PET cortical mean
Tau PET cortical mean
Tau PET cortical mean
Tau PET cortical mean
Tau PET cortical mean